Scale matters: the influence of structural inheritance on fracture patterns

Anindita Samsu[1], Alexander R. Cruden[1], Steven Micklethwaite[1], Lachlan Grose[1], Stefan A. Vollgger[1]

[1]*School of Earth, Atmosphere and Environment, Monash University, Clayton, VIC 3800, Australia*

This manuscript is a non-peer-reviewed preprint submitted to
Journal of Structural Geology

Scale matters: the influence of structural inheritance on fracture patterns

Anindita Samsu[1*], Alexander R. Cruden[1], Steven Micklethwaite[1], Lachlan Grose[1], Stefan A. Vollgger[1]

[1]School of Earth, Atmosphere and Environment, Monash University, Clayton, VIC 3800, Australia

*Corresponding author: anindita.samsu@monash.edu

Keywords: fractures, structural inheritance, rift basin, Gippsland Basin

ABSTRACT

Fracture systems are often geometrically invariant across a range of scales, but the impact of structural inheritance on this pattern is poorly understood. This paper shows how fracture orientations in sedimentary rocks vary at different scales when influenced by pre-rift basement structures. We use high-resolution unmanned aerial vehicle (UAV) orthophotos to map folds and fractures in the basement and cover rocks of the Gippsland Basin, southeast Australia. Outcrop-scale observations are compared with >1 km long faults previously interpreted from potential field geophysics data. We use length-coloured rose diagrams of fracture traces to compare trends in fracture orientations. Early Cretaceous syn-rift normal faults exhibit the same ENE-WSW trend at basin and outcrop scale. Pervasive outcrop-scale NNW-SSE joints record a subsequent regional shortening event, but at the basin scale this is only expressed as reverse reactivated ENE-WSW striking faults. Thus, fabrics and/or faults in the underlying basement exert significant control on the orientation of basin-scale fractures in

the cover but appear to have limited influence on outcrop-scale fracture orientations. Our observations show that fracture systems influenced by structural inheritance are not scale-invariant, and that a proper understanding of structural architecture can only be achieved by analysing data that span multiple scales.

1. INTRODUCTION

The formation of fractures in a rift basin is primarily controlled by far-field stresses resulting from active tectonic processes. However, pre-existing mechanical heterogeneities in pre-rift "basement" rocks can interact with the far-field stress during the evolution of the rift basin, influencing the formation of fractures in the sedimentary "cover" rocks ("structural inheritance"). For example, multiple studies on rift systems (e.g., Morley et al., 1990; Corti et al., 2007) demonstrate that local stress perturbations in the vicinity of pre-existing structures can significantly alter stress trajectories, affecting the orientation and geometry of new fractures (Bourne and Willemse, 2001; Maerten et al., 2002; de Joussineau et al., 2003; Morley, 2010). Pre-existing faults or shear zones in the basement of a basin can be "inherited" by the overlying sedimentary cover through fault reactivation (Kirkpatrick et al., 2013; Phillips et al., 2016), which results in parallelism or "geometric similarity" between a reactivated basement structure and a newly formed cover fault (Holdsworth et al., 1997). Structural inheritance can also be recognized when the trend of cover fractures appear to change across areas that overlie different basement domains even when the fractures do not directly link into the basement structures (Wilson et al., 2010; Samsu et al., 2019). This second mechanism of inheritance is a poorly understood phenomenon that nevertheless can have a significant impact on fracture orientations and connectivity.

While it is widely accepted that structural inheritance can impact the orientation of entire rifts as well as smaller-scale faults within rift basins (e.g., Corti et al., 2007; Henza et al., 2011;

Reeve et al., 2015), few studies examine the influence of inheritance on the formation of fractures in one study area at multiple scales. In a study of the northeast Brazilian margin, Kirkpatrick et al. (2013) found that the orientation of regional rift faults are parallel to sub-vertical, crustal-scale shear zones in the basement – which could be attributed to reactivation of the basement shear zones during rifting (Phillips et al., 2016) – while syn-rift outcrop-scale faults are oblique to the shear zones and the pervasive basement fabric. Their findings suggest that the influence of pre-existing basement structures is scale-dependent. However, it is rarely the case that structures in basement rocks can be compared with the overlying cover rocks at the same scale. The interpretation of faults in cover rocks is usually conducted on seismic reflection data (e.g, Peace et al., 2017; Phillips et al., 2016; Reeve et al., 2015), while basement structures at the margins of rift basins are observed in outcrops (e.g., Kirkpatrick et al., 2013).

Our study uses the Cretaceous western onshore Gippsland Basin (southeast Australia; Fig. 1) as a natural laboratory to investigate how pre-existing discrete faults and a pervasive fabric in the basement may have influenced fracture orientations in the overlying cover rocks. The onshore Gippsland Basin provides a unique opportunity to study the various scales at which inheritance operates. Firstly, the two known levels of basement underneath the basin – a Paleozoic and a Neoproterozoic-Cambrian basement – allow us to study multiple orders of inherited structures. Secondly, onshore exposure of basement and cover rocks along the coast allow us to directly compare structures in basement and cover rocks at the same scale.

<Insert Figure 1 here>

We used high-resolution unmanned aerial vehicle (UAV) orthophotos of outcrops to map pre-existing structures in the basement and thousands of fractures in the cover rocks. Maps of fracture traces (including faults and joints) and orientation statistics of fracture data were

used to separate regional fracture trends from local trends. In this paper, we compare existing interpretations of basin-scale (>1 km scale) faults with the outcrop-scale fracture data. Using field observations, we present possible hypotheses of how discrete discontinuities or pervasive mechanical anisotropies in the basement, such as bedding, fold axial planar foliations, faults, and rheological boundaries, affect deformation in the cover rocks during the syn-rift and post-rift (inversion) stages of basin development. Our findings show that the orientations of fractures that have been influenced by pre-existing basement structures vary between scales of observation.

2. GEOLOGICAL SETTING

The Gippsland Basin is part of the Australian Southern Margin rift system, which formed during Jurassic–Cretaceous rifting between Australia and Antarctica (Miller et al., 2002 and references therein). Overall, the basin is characterized by three main sets of rift-related faults. NE-SW and ENE-WSW trending reverse-reactivated normal faults are dominant in the western onshore part of the basin. The eastern onshore part of the basin is populated by roughly E-W trending faults, and the offshore part contains WNW-ESE to NW-SE trending normal faults (Willcox et al., 1992).

Rifting in the Gippsland Basin began in the Early Cretaceous (Fig. 2), first forming syn-depositional normal faults in the onshore Gippsland Basin that trend NE-SW to E-W (Willcox et al., 1992) (Fig. 1). Rifting was interrupted by a period of uplift and inversion at the end of the Early Cretaceous (Dumitru et al., 1991; Duddy and Green, 1992; Foster and Gleadow, 1992; Willcox et al., 1992; Samsu et al., 2019). This event was associated with NNW-SSE oriented compression, which formed NE-SW and ENE-WSW trending reverse faults and anticlines along reactivated rift-related normal faults in the onshore part of the basin (Norvick and Smith, 2001). Rifting then resumed and continued into the Late

Cretaceous, during which time E-W to NW-SE trending rift-related faults (e.g., the Rosedale and Foster fault systems; Fig. 1) formed in the eastern onshore and offshore Gippsland Basin (Power et al., 2003). The post-rift Cenozoic history records additional tectonic episodes associated with compression and a NNW-SSE oriented maximum horizontal stress. The stress state has not changed significantly since this time, as the present-day in-situ stress is characterized by a NW-SE oriented (130 ± 20°) maximum horizontal stress (Hillis and Reynolds, 2000).

<Insert Figure 2 here>

NE-SW and ENE-WSW trending syn-rift faults in the Early Cretaceous Strzelecki Group of the western onshore Gippsland Basin (Samsu et al., 2019; Fig. 3) are oblique to the inferred N-S to NNE-SSW regional extension associated with the Early Cretaceous rifting of the Otway and Gippsland basins (Etheridge et al., 1985; Willcox et al., 1992; Hill et al., 1994, 1995; Chantraprasert et al., 2001; Norvick et al., 2001; Miller et al., 2002; Krassay et al., 2004). This obliquity suggests the influence of the underlying anisotropic, heterogeneous basement rift faulting. This paper discusses the interaction between the two basement units underneath the Gippsland Basin – the folded and faulted Paleozoic basement and a deeper Neoproterozoic–Cambrian basement – and the syn-rift Lower Cretaceous Strzelecki Group cover rocks that unconformably overlie the basement. The following sections provide a brief overview of the geology and structural trends within these three units.

<Insert Figure 3 here>

2.1 Cretaceous cover rocks

Rocks of the Lower Cretaceous Strzelecki Group are exposed in cliffs and wave-cut platforms along the coastline near San Remo and in the Cape Paterson area (Fig. 3). These outcrops comprise alternating layers of mud-dominated and sand-dominated siliciclastic

rocks with conglomeritic or organic matter-rich interbeds, which were deposited in a fluvial setting (Constantine, 2001). Dip angles of bedding are low, varying between 6° and 26° (Aghaei et al., 2017). High-angle changes in the strike of bedding occur across faults, some of which extend seawards beyond the wavecut platforms, where they can be interpreted from bathymetry data (Samsu et al., 2019). NW-SE to NNW-SSE trending dolerite dikes of Cretaceous age (Duddy and Green, 1992; Constantine, 2001; Samsu et al., 2019) crosscut the Strzelecki Group.

2.2 The Paleozoic basement

The western onshore part of the Gippsland Basin is underlain by Paleozoic rocks of the Melbourne Zone of the Lachlan Orogen, while the eastern onshore and offshore parts lie above the Tabberabbera, Kuark, and Mallacoota Zones (VandenBerg et al., 2000) (Fig. 1). Major faults and fold axial traces in the Melbourne Zone trend predominantly NNW-SSE as a result of folding and thrusting associated with E-W shortening during the Tabberabberan Orogeny (VandenBerg et al., 2000). An exception to this structural trend is the northern part of the Melbourne Zone, where E-W trending faults and fold axial traces may indicate an episode of N-S shortening that postdates the E-W shortening (VandenBerg et al., 2000). In southern Victoria, a large portion of the Melbourne Zone is mostly covered by Cretaceous to recent sediments of the Gippsland Basin. However, a NNE-SSW structural trend can be observed in Ordovician rocks that crop out on the Mornington Peninsula and Devonian rocks that are exposed at Cape Liptrap (Keetley et al., 2001; Cayley et al., 2002; Vollgger and Cruden, 2016) (Fig. 3).

Exposed Paleozoic faults trend NNE-SSW (Gray et al., 1999; Cayley et al., 2002), such as the Waratah Fault, Bell Point Fault, and Selwyn Fault (Fig. 1). The Waratah Fault, which is exposed along the southeastern side of Cape Liptrap, has been reactivated multiple times, up

until the Holocene (Gardner et al., 2009). The seismically active Selwyn Fault follows the western margin of the Mornington Peninsula (Fig. 3) (Willcox et al., 1992; Cayley et al., 2002). Because of the high contrast in the magnetic characteristics of the rocks on either side of the Selwyn Fault and the length of the fault, it is interpreted that this structure links down into older faults in the Neoproterozoic–Cambrian basement that were active during the Cambrian Tyennan Orogeny (Cayley et al., 2002). The spacing between these deep crustal faults is relatively wide – for example, the Waratah Fault and Selwyn Fault are ~100 km apart.

2.3 The Neoproterozoic–Cambrian basement

The Paleozoic Melbourne Zone unconformably overlies the Neoproterozoic–Cambrian Selwyn Block (Cayley et al., 2002; McLean et al., 2010) (Fig. 1). Folds in the Melbourne Zone, which formed during the Tabberabberan Orogeny, have longer wavelengths and lower amplitudes than those in the adjacent zones, to the west and east, respectively. Therefore, it has been inferred that the underlying Selwyn Block is more rigid than the surrounding lower crust and that it shielded the Melbourne Zone from extensive deformation (VandenBerg et al., 2000).

The Selwyn Block comprises metasedimentary and metavolcanic rocks of Neoproterozoic–Cambrian age that were accreted onto the east Gondwanaland margin during the Late Cambrian Delamerian Orogeny (Cayley, 2011). The Cambrian minimum age for regional deformation is defined by an unconformity above Selwyn Block rocks, which crop out at several locations, including at Cape Liptrap (Cayley et al., 2002; VandenBerg et al., 2006). The Selwyn Block comprises several lithological and structural units, as indicated by N-S to NE-SW trending magnetic anomalies (Moore et al., 2016). In south-central Victoria a steeply SW-dipping, NW-trending fault displaces Devonian rocks against Cambrian rocks, which has

168 been interpreted as a Cambrian fault that underwent reactivation during the Tabberabberan
169 Orogeny (ca. 380 Ma; Gray and Willman, 1991). The eastern boundary of the Selwyn Block
170 and internal fabrics within the study area trend NE-SW (Fig. 1).

171 ## 3. METHODS

172 A multi-scale structural mapping approach was employed to identify correlations between
173 structures in basement and cover rocks. In this study, "fractures" include shear fractures and
174 joints, all of which form when rocks fail in a brittle manner. The term "fault" is used to
175 describe a zone comprising linked segments of shear fractures when the individual shear
176 fractures cannot be recognized at the scale of observation. "Fracture zone" is used for areas of
177 intensely fractured rock, which in wavecut platforms have typically been eroded. The term
178 "joint" is used to describe a fracture that exhibits no offset along its length at the scale of
179 observation. Fractures are considered systematic when they are parallel or sub-parallel or are
180 regularly distributed, hence a fracture set consists of parallel to sub-parallel systematic
181 fractures. Irregularly oriented fractures that demonstrate no obvious spatial relationship to
182 one another are considered to be non-systematic.

183 Outcrop-scale mapping of basement structures were conducted on Melbourne Zone outcrops
184 at Shark Stack (Cape Liptrap, see Fig. 3 for location). Although Cambrian metavolcanic
185 rocks of the Selwyn Block are exposed nearby (Cayley et al., 2002), the highly deformed
186 nature of the outcrop made it unsuitable for collecting structural measurements. Structures at
187 the Shark Stack locality were interpreted from field observations, with the help of
188 orthophotos generated from aerial photographs collected from an unmanned aerial vehicle
189 (UAV) (Vollgger and Cruden, 2019). Previous mapping of basin-scale (>1 km-scale) faults
190 using gravity and magnetic data (Samsu et al., 2019), help to constrain general structural
191 trends and distinguish between pre-rift and syn-rift structures in the basement. Fractures in

cover rocks in the Cape Paterson area (see Fig. 3 for location) were traced semi-automatically from UAV orthophotos, which facilitated rapid collection of data on thousands of fractures over a wide area at high spatial resolution. Here we introduce the workflow used for collecting fracture data and for evaluating trends in the orientation of fracture traces.

3.1 Semi-automated fracture tracing

UAV-derived orthophotos of outcrops enabled the collection of fracture data at five outcrop localities (Fig. 4) over a total area of ~0.934 km^2. These orthophotos are suitable for evaluation of fracture variability and clustering across a wide area using the areal sampling method, where fracture traces are mapped in two dimensions (2D) using aerial photographs (Wu and D. Pollard, 1995; Watkins et al., 2015). As the individual mapped areas were relatively large (up to 0.330 km^2), the likelihood for sampling bias at each map locality – which can be problematic when fracture patterns change with position (Rohrbaugh et al., 2002) – could be reduced. For a summary of the UAV photogrammetry workflow and the parameters chosen for the UAV surveys, see Table 1 in the supporting information (cf. Dering et al., 2019).

<Insert Figure 4 here>

Fractures at the five outcrop localities – Harmers Haven North, Harmers Haven South, Eagles Nest, The Caves-Flat Rocks, and Inverloch (Fig. 4) – were interpreted using a semi-automated fracture tracing method (Fig. 5). The method, implemented as a QGIS plugin, GeoTrace (Thiele et al., 2017), uses a least-cost path algorithm on a cost function that highlights geological features. We traced fractures that were visible at one chosen scale of 1:500 (Fig. 6). We found that tracing fractures at this scale provided a good balance between maximizing the use of the high-resolution orthophotos (down to 1.94 cm/pixel) and limiting the amount of time required to trace all of the observable fractures (up to eight hours for one

locality). Our method ensured that when we analysed the orientation of the fracture populations from different localities, we were comparing fractures that were observable at the same scale.

<Insert Figure 5 here>

<Insert Figure 6 here>

3.2 Fracture orientation analysis using length-coloured rose diagrams

Circular histograms, or rose diagrams, are common statistical plots for analysing the orientation distribution of fractures within a study area (e.g., Marchegiani et al., 2006; Munro and Blenkinsop, 2012; Lavenu et al., 2013; Healy et al., 2016). Unweighted rose diagrams are calculated without discrimination between fractures of different lengths. Weighted rose diagrams are typically calculated by weighting the influence of a fracture's orientation by the fracture length. An alternative to binned rose diagrams are Gaussian smoothed rose diagrams (e.g., Robin and Jowett, 1986), which are useful for accentuating trends in orientation data. While these existing variations of rose diagram types help to identify fracture orientation trends, none of them show the length of the fractures that make up each trend in a rose diagram.

In this study, we are interested in the contribution of fractures of different lengths to fracture orientation trends within each outcrop area. Our approach is concerned with whether fractures of different lengths develop different orientations preferentially, therefore testing for scale-dependence. Fracture traces that are relatively long are often straight, continuous joints that have not been offset by subsequent shear fractures. Alternatively, they can represent larger faults, where individual shear fracture segments cannot be recognized at the scale of observation, either due to the close spacing between segment tips or weathering along the

fracture. Shorter fracture traces mostly represent joints, shear fractures, or non-systematic fractures.

Here we present a new technique for characterizing the trends in a fracture population, where the distribution of fracture lengths are plotted on an unweighted rose diagram to produce "length-coloured rose diagrams." These rose diagrams allow for a more comprehensive analysis of the fracture network, showing whether each peak orientation is associated with relatively "short" or "long" fracture traces. The petals of the rose diagram are subdivided into coloured segments that represent the percentage contribution of fractures within each length bin. This method has been implemented in the GeoTrace plugin for QGIS (Thiele et al., 2017; QGIS Development Team, 2019). Fracture orientations were compared between the five different outcrop localities (Fig. 4 and 5). For each locality, all of the fractures that were traced at a scale (or 'zoom') of 1:500 were treated as one population, resulting in one rose diagram per locality.

3.3 Fracture orientation analysis using gridded rose diagrams

A second analysis was performed to assess the heterogeneity of fracture patterns within individual outcrop localities, as there is usually significant variation in fracture density or orientations even within a small area. For the Harmers Haven North locality (see Fig. 4 for location), fractures were traced manually at a scale of 1:500. Grid tiles with 100 m by 100 m dimensions were overlain onto the fracture trace map, and a length-weighted binned rose diagram (with 10°-wide bins) was generated for the fracture trace segments in each grid tile, resulting in one rose diagram per grid tile (Fig. 7). Grid tiles that contained less than 30 fracture trace segments were excluded from the analysis. This technique is implemented in the Line Direction Histogram plugin (Tveite, 2015) for QGIS. This method allowed us to test the consistency of fracture orientations throughout an outcrop. It also assisted in determining

whether clustering or anomalous fracture patterns in a given locality are associated with changes in lithology, structural style, or other factors.

<Insert Figure 7 here>

4. RESULTS

4.1 Structural characteristics of basement rocks (Cape Liptrap)

The Shark Stack outcrop is located near the southwestern tip of Cape Liptrap (Fig. 8). Here, tightly folded turbidites of the Devonian Liptrap Formation are exposed on wavecut platforms and steep, SSW-facing cliffs (Fig. 9 and 10). The rocks comprise steeply dipping, alternating beds of sandstone and mudstone, and they exhibit a first-order NNE-SSW structural trend in map view (Fig. 8c). The sequence of ductile and brittle deformation inferred for the Shark Stack locality is summarized in Table 1, interpreted using observations acquired from both field and UAV-based mapping of structures.

<Insert Figure 8 here>

<Insert Table 1 here>

The strike of bedding in the fold limbs is predominantly NNE-SSW, with beds dipping steeply to sub-vertically towards the ESE and WNW (Fig. 9d). The fold axis calculated from bedding measurements (from across the entire outcrop) trends 198° and plunges 20°, which represents the fold axis of the first-generation F1 folds at this locality. This fold axis is consistent with the F1 fold axis reported for the southern part of Fold Stack (201/11; Vollgger and Cruden, 2016). A steeply ESE-dipping to sub-vertical, axial planar cleavage is consistent with the bedding measurements and fold axis, suggesting that local shortening was WNW-ESE. We interpret the F1 folds in the area to be related to ~E-W shortening associated with the Devonian Tabberabberan Orogeny (385 – 380 Ma; VandenBerg et al., 2000). Reverse

faults with a low strike angle to bedding offset sandstone beds, while associated strain is accommodated by ductile deformation of the mudstone layers.

<Insert Figure 9 here>

The Shark Stack outcrop contains N-S trending zones of intensely folded beds (Fig. 10). In map view, these structures appear to be either reverse kink bands or disharmonic folds (Fig. 10a), though cross section (along subvertical cliffs) they appear exclusively as disharmonic folds (Fig.10b). Kink band formation in some zones has progressed to chevron folding. Similar “kink folds” have been observed in shale-rich outcrops at the southernmost tip of Cape Liptrap, ~800 m southeast of Shark Stack. Axial traces of folds within these zones, mapped on the UAV orthophoto, trend predominantly N-S (Fig. 10a), oblique to the first-order F1 fold axis. Fold hinges plunge mostly to the south (Fig. 9f), consistent with axial traces mapped on the 2D dataset. We attribute these second-order F2 folds to a separate D2 folding event associated with NNE-SSW compression, sub-parallel to the strike of bedding. This interpretation is based on analogue experiments, field examples, and mechanical experiments of kink bands in anisotropic media, which suggest that reverse kink bands result from local shortening parallel to the anisotropy (e.g., Cobbold et al., 1971; Stubley, 1989; Kapp et al., 2016) (e.g., Cobbold et al., 1971; Stubley, 1989). Based on observations at Shark Stack, it is possible that the N-S trending fractures at Fold Stack are shear fractures that formed at an acute angle to NNE-SSW directed compression during late stages of kink band development (cf. Vollgger and Cruden, 2016). Field evidence for N-S to NNE-SSW compression – including E-W trending folds, north-dipping reverse faults, and steeply dipping, E-W striking axial planar cleavage – at a later stage of the Tabberabberan Orogeny (following E-W compression) has also been found in the northern part of the Melbourne Zone (Gray and Mortimer, 1996; Wilson et al., 2017).

<Insert Figure 10 here>

ENE-WSW trending dextral shear fractures and a larger fracture zone of the same orientation (Fig. 8c) is attributed to a D3 brittle deformation event. Like the ENE-WSW trending fracture set at Fold Stack (Vollgger and Cruden, 2016), this set is parallel to Early Cretaceous rift-related normal faults within the Lower Cretaceous Strzelecki Group (Samsu et al., 2019). They are the only structures at Shark Stack that can be associated with Early Cretaceous Gippsland Basin rifting.

A D4 deformation event is associated with a NW-SE trending kink band zone that extends across the middle and along the length of the entire Shark Stack outcrop, overprinting F2 kink bands (Fig. 8c and 10). In this <3.3 m wide zone, the local sense of shear is dextral, and the kinks offset the sandstone and mudstone layers laterally by <1 m. Smaller, less developed kink bands of the same orientation are also present. A NNW-SSE trending set of sinistral fractures occurs in the northwest section of the outcrop (Fig. 8c). The acute bisector between the F4 kink bands and the NNW-SSE fractures is ~30°. Based on the orientation and kinematics of the F4 kink bands and the NNW-SSE trending fracture set, we interpret them as conjugate structures that formed during a phase of NNW-SSE directed D4 shortening. The relative timing of D3 fractures and D4 kinks is ambiguous – the large ENE-WSW trending fracture zone potentially offsets NW-SE trending kink bands in the orthophoto (Fig. 8c), but the amount of weathering in this part of the outcrop makes it difficult to confirm this. As the two sets are orthogonal to each other and both exhibit a dextral sense of movement, they cannot have formed coevally.

Most of the NW-SE trending structures at Shark Stack that were mapped using the UAV orthophoto are short F4 kink bands (<10 m in length) (Fig. 11). Longer fractures (>10 m) are associated with NNW-SSE and ENE-WSW trending fracture sets. These fractures are

relatively young D3 and D4 structures compared to pre-rift D1 and D2 structures and show high lateral continuity because they have not been overprinted by younger structures.

<Insert Figure 11 here>

4.2 The orientation of fractures in cover rocks (Cape Paterson area)

Fracture orientation trends in the Strzelecki Group cover rocks in the Cape Paterson area (see Fig. 3 for location) are presented as rose diagrams (Fig. 4 and 5) and summarized in Table 2. Here we describe fracture orientations at five outcrop localities – Harmers Haven North, Harmers Haven South, Eagles Nest, the Caves – Flat Rocks, and Inverloch – and use peaks in the data to classify fracture traces into fracture sets. We also use overprinting relationships between fracture traces in the UAV orthophotos and field observations to identify the type of fractures that make up each fracture set.

<Insert Table 2 here>

The predominant trend at Harmers Haven North is NNW-SSE (335–350°) (Fig. 5a). This fracture set comprises linear, systematic joints that are parallel to – and are potentially exploited by – NNW-SSE trending mafic dikes. We observe two other peaks in the data for this locality: WNW-ESE (280–295°) and E-W (80–100°), which correspond to shear fractures. These two sets are more prevalent in the central part of the outcrop, while the NNW-SSE trending set is more dominant in the western and eastern parts of the outcrop. The longer (>30 m) fracture traces at this locality are faults across which the strike of bedding changes significantly. A more detailed discussion of the spatial variability of fracture trends at Harmers Haven North (Fig. 7) is presented below.

At Harmers Haven South, one wide peak in the rose diagram is present, trending NNW-SSE (325-345°) (Fig. 5d). The NNW-SSE fracture set consists mostly of joints, some of which are

exploited by NNW-SSE trending mafic dikes at the northern end of the outcrop. Faults trend NW-SE and some of them are also exploited by NW-SE trending mafic dikes.

The Eagles Nest locality was split into a southern and northern area (Fig. 5b). The rose diagram of fracture traces in both areas combined show a dominant NNW-SSE (325-345°) peak. The second most dominant trend is represented by a wide peak, trending ENE-WSW (65-80°) and E-W (80-95°). In the southern area, NNW-SSE and ENE-WSW trending systematic fracture sets, which are mutually crosscutting, are present near the Eagles Nest pinnacle. The ENE-WSW trending normal fault slightly north of the pinnacle is associated with Early Cretaceous rifting. A NE-SW trending fracture set is confined to a small area west of the pinnacle. In the northern area, a large N-S trending fracture zone bounds the Eagles Nest locality to the east. The N-S trending fault truncates an ENE-WSW trending fault and the NNW-SSE fracture set to the west. The significant rotation of sedimentary beds across this fault and the syn-sedimentary nature of ENE-WSW trending normal faults in the area (Samsu et al., 2019) suggests that the N-S fault postdates ENE-WSW normal faulting.

At the Caves – Flat Rocks, the main peak in the rose diagram corresponds to NNW-SSE (320–345°) trending shear fractures (Fig. 5e). The second-most dominant peak is associated with ENE-WSW (65–85°) trending fractures, some of which are normal faults associated with Early Cretaceous rifting. A third, less dominant NNE-SSW (10-20°) trend is made up of shear fractures. ENE-WSW trending faults are offset by NNW-SSE and NNE-SSW trending shear fractures, which may explain why this fracture set has the highest percentage of shorter (<10 m) fractures relative to their frequency. The Inverloch locality is populated by fractures that are shorter than 20 m (Fig. 5c). One sharp E-W trending peak (85 – 95°) and another sub-population of WNW-ESE to NNW-SSE (290 – 345°) trending fractures are represented in the rose diagram.

A common occurrence among the five described localities is the presence of a NNW-SSE trending fracture set, which mostly consists of sub-vertical joints. This joint set is interpreted to be a pervasive, regional outcrop-scale joint set that reflects Early Cretaceous shortening (Samsu et al., 2019), which postdates Early Cretaceous syn-rift normal ENE-WSW faulting and predates the Aptian intrusion of NW-SE and NNW-SSE trending mafic dikes in the study area. The formation of this joint set could also be coeval with reverse reactivation of the optimally oriented, aforementioned ENE-WSW trending normal faults, which agrees with an interpretation by Power et al. (2003) of similarly orientated compressional structures in the offshore Gippsland Basin.

4.2.1 Variability of fracture orientations within the Harmers Haven North locality

The Harmers Haven North outcrop was subdivided into three domains based on the main fracture orientations (Table 2; Fig. 7). The western section of the outcrop (Domain A) exhibits a dominant NNW-SSE trending fracture set. Field observations confirm that this set is made up of joints, similar to the NNW-SSE trending fracture set at Harmers Haven South. Domain A also contains a single NNW-SSE trending dike that is parallel with the main joint set. A less prominent E-W trending fracture set is present in Domain A. The middle section of the outcrop (Domain B) does not exhibit a dominant fracture set. It contains a dense network of non-systematic shear fractures. Three of the NNE-SSW trending shear fractures in Domain B (represented by thick red lines in Fig. 7) correspond to km-scale faults interpreted from near-shore bathymetry (Fig. 4). The eastern section of the outcrop (Domain C) exhibits the same NNW-SSE joint set as observed in Domain A, although fractures of other orientations are also present.

4.2.2 Curved fractures at the Eagles Nest locality

The most dominant fracture set at Eagles Nest is the NNW-SSE trending set of up to 50 m long fractures (Fig. 12). NNW-SSE trending fractures in the northern area curve eastwards into the N-S trending fracture zone. There is no evidence of shear along these NNW-SSE trending fractures, so they can be interpreted as joints, like the NNW-SSE trending joints at Harmers Haven North and Harmers Haven South (Table 2). The curved NNW-SSE joints at Eagles Nest are comparable with joints that "veer" from linearity (Cruikshank and Aydin, 1995) as they propagate into a changing stress field, which may result from stress perturbations near pre-existing structures. Photoelastic experiments on analogue materials (e.g., de Joussineau et al., 2003) demonstrate the deviation of stress trajectories near pre-existing defects (analogous to faults in rocks) under a biaxial compressive load. Welch et al. (2014) discuss the development of local stress anomalies near tips, bends and splays in larger faults. At Eagles Nest, veering of the NNW-SSE joints would have resulted from the divergence of local maximum principal stress trajectories from the regional compression, which was due to local stress perturbations around the large N-S trending fracture zone.

<Insert Figure 12 here>

4.3 Basin-scale fracture trends

The length-coloured rose diagram of regional fault traces shows that large, regional faults exhibit a range of trends between N-S and ENE-WSW (Fig. 3). The interpretation of the timing of these faults and their orientations are outlined in Samsu et al. (2019). ENE-WSW trending faults are Early Cretaceous rift related faults that were reactivated during Early Cretaceous NNW-SSE directed compression, which was also responsible for NNW-SSE jointing at Harmers Haven and Eagles Nest. N-S to NNE-SSW trending faults crop out along the coast between Harmers Haven and Inverloch and appear as up to ~20 m wide fracture zones in near-shore bathymetry data (Fig. 4). Similarities in their orientation and kinematics

428 with pre-rift basement faults, such as the Waratah Fault and Selwyn Fault (Gray et al., 1999;
429 Gardner et al., 2009; Samsu et al., 2019), suggest that they could have formed in association
430 with reactivation of NNE-SSW trending basement fractures.

431 ## 5. DISCUSSION

432 ### 5.1 Rift faults oblique to basement structures and the regional extension direction

433 Basement reactivation results in new faults that are parallel to pre-existing basement
434 structures (e.g., Holdsworth et al., 1997; Kirkpatrick et al., 2013; Phillips et al., 2016). In the
435 western onshore Gippsland Basin, NNE-SSW trending faults in the Neoproterozoic–
436 Cambrian Selwyn Block basement were reactivated during Devonian deformation of the
437 shallower Melbourne Zone basement, forming the Waratah and Selwyn faults. In contrast to
438 these contractional structures, normal Cretaceous syn-rift faults in the study area trend NE-
439 SW and ENE-WSW, oblique to pre-existing NNE-SSW trending structures. These normal
440 faults are also oblique to their expected E-W orientation given the inferred N-S regional
441 extension. These observations suggest that a mechanism other than reactivation may be
442 responsible for inheritance influenced syn-rift normal faulting (Fig. 13b). Reactivation of
443 basement structures ought to have resulted in NNE-SSW trending normal faults that are
444 parallel to pre-existing basement structures.

445 <Insert Figure 13 here>

446 Existing research on inheritance in rift basins largely focuses on reactivation (e.g., Whipp et
447 al., 2014; Phillips et al., 2016; Fazlikhani et al., 2017; Collanega et al., 2019; Heilman et al.,
448 2019). However, we suggest a second, poorly understood mechanism of structural inheritance
449 involves a rotation of the stress field above an anisotropic basement unit with a structural
450 trend that is oblique to the rifting direction. Our observations are comparable with the results
451 of field studies from north-western Scotland (Wilson et al., 2010) and the East African rift

system (Morley, 2010), where fracture orientations vary between areas that have different basement domains. Changes in fracture orientations are attributed to local re-orientation of the far-field, regional stress field above pre-existing basement fabrics that are oblique to the main rift trend (Morley, 2010), and direct reactivation of basement structures is not required for the basement to influence faulting in the cover in this way (Wilson et al., 2010).

5.2 The influence of multiple levels of basement on cover faults

Two orders of basement beneath the western Gippsland Basin study area likely had an impact on basin formation (Fig. 1). Both levels of basement were subjected to multiple shortening events prior to Early Cretaceous rifting and opening of the Gippsland Basin, resulting in a first-order NNE-SSW structural trend (Gray et al., 1999; Cayley et al., 2002; McLean et al., 2010; Moore et al., 2016) that is oblique to subsequent Cretaceous rift-related structures. NNE-SSW trending faults in the Melbourne Zone formed as a result of roughly E-W shortening during the Devonian Tabberabberan Orogeny. Some of these faults, such as the Waratah and Selwyn faults, extend into the underlying Selwyn Block basement, so it has been suggested that reactivation of Selwyn Block faults exerted some control on Devonian deformation in the Melbourne Zone basement (Cayley, 2011) (A in Fig. 13a).

Based on field observations of NNE-SSW trending D1 structures at Shark Stack and Fold Stack (Vollgger and Cruden, 2016) (Cape Liptrap; Fig. 9), we infer that the Melbourne Zone underneath our study area exhibits a penetrative NNE-SSW trending anisotropy. The mechanical anisotropy created by alternating mudstone and sandstone units has the potential to locally perturb the far-field stress. Alternatively, relatively weak mudstone layers between competent sandstone layers may be prone to re-shearing when the crust is subject to later extension or compression. This anisotropy should have exerted a greater influence on

475 regional faulting patterns in the cover compared to less pervasive, more localized fractures (B
476 in Fig. 13a).

477 The postulated eastern boundary of the Selwyn Block (and the overlying Melbourne Zone)
478 coincides with a change from NE-SW and ENE-WSW trending faults in the western onshore
479 part of the Gippsland Basin to E-W trending faults in the eastern onshore and offshore parts
480 (Cayley et al., 2002) (Fig. 1). The lower crustal Selwyn Block is inferred to be more rigid
481 than the surrounding lower crust (Cayley et al., 2002; Teasdale et al., 2004), so that the
482 Selwyn Block boundary separates an anomalously strong lower crustal block from the
483 "normal" lower crust. The strength contrast between the Selwyn Block and the adjacent,
484 weaker, lower crust could be an additional source of stress re-orientation that contributed to
485 the non-parallelism of the rift faults in the cover (C in Fig. 13a).

486 **5.3 Structural inheritance is not scale-invariant**

487 Multi-scale mapping of fracture traces allowed comparison between: 1) the orientations of
488 outcrop-scale basement and cover structures, and 2) the orientations of basin-scale (>1 km-
489 scale) fractures and outcrop-scale (meters to tens of meters-scale) fractures. By comparing
490 D3 and D4 basement structures with cover fractures, we observed that a single tectonic event
491 can be reflected by different fracture trends in basement and cover rocks, likely due to
492 differences in the mechanical anisotropy. Outcrop-scale cover fractures in our study area
493 have trends that are different to outcrop-scale basement fractures, with the exception of the
494 ENE-WSW trending fracture set (Fig. 3 and 4). Syn-rift normal faults exhibit the same ENE-
495 WSW trend at both basin scale and outcrop scale (Fig. 14a).

496 <Insert Figure 14 here>

497 The trends of outcrop-scale fractures that formed during NNW-SSE directed regional
498 compression are different from the trends of basin-scale fractures (Fig. 14b). The persistent

NNW-SSE peak in the outcrop-scale fracture data highlights the abundance and pervasiveness of a NNW-SSE trending subvertical joint set in the Strzelecki Group cover rocks across the entire study area. Samsu et al. (2019) have discussed the formation of this joint set under NNW-SSE directed maximum horizontal stress, coeval with a conjugate set of NNW-SSE and N-S to NNE-SSW trending strike-slip faults, which may coincide with Early Cretaceous (Aptian) basin uplift and the reverse reactivation of ENE-WSW rift faults (Holdgate et al., 2003; Power et al., 2003). While NNW-SSE trending joints formed at the small scale during NNW-SSE contraction, ENE-WSW trending normal faults were reactivated at the large scale, so that the NNW-SSE trend is absent in the rose diagram for the basin-scale fracture traces (Fig. 3 and 14b). This event could have also reactivated optimally oriented NNE-SSW trending basement faults in a strike-slip sense, which explains the NNE-SSW fracture trend in the rose diagram for basin-scale faults (Fig. 14b).

At outcrop scale, NNW-SSE trending joints behave differently near large faults that either pre-date or are coeval with joint formation. At Eagles Nest, the joints veer into perpendicularity with a large N-S trending fracture zone that may have locally perturbed far-field stress trajectories (Fig. 12). This joint set is absent adjacent to NNE-SSW trending faults at Harmers Haven North.

In our study area, joints formed at the small scale, but reverse reactivation of normal faults occurred at the large scale. Our results imply that small-scale fractures do not represent large-scale fractures when the basement influence is strong. Pervasive, small-scale joints may be faithful recorders of the far-field stress when not affected by adjacent larger faults, which serve to alter the local stress field.

6. CONCLUSIONS

Pre-existing basement structures exert significant control on the orientation and distribution of fractures in the sedimentary cover rocks of a rift basin. However, this basement influence manifests itself differently at different scales. Inheritance does not always result in cover fractures that are parallel to basement structures, which is expected with basement reactivation. In the western onshore Gippsland Basin, both basin-scale and outcrop-scale syn-rift faults are oblique to the basement trends as well as their expected orientation based on the known far field extension direction, suggesting that stresses above the basement structures were rotated such that faults in the cover rocks became misaligned to both their expected orientation and the basement anisotropy. This finding should motivate us to explore and model the mechanisms of structural inheritance, other than reactivation, through additional field-based studies as well as analogue and numerical experiments.

When attempting to understand the influence of structural inheritance on deformation in a rift basin, it is important to consider not just the basement that directly underlies the sedimentary cover, but older, deeper basement units as well. As multiple levels of basement are often present, it is challenging to distinguish the relative contributions of pre-existing structures from each basement unit. In our study area, widely-spaced faults in the deeper Neoproterozoic–Cambrian Selwyn Block basement were reactivated during Devonian deformation of the shallower Melbourne Zone basement. Because these faults appear to have been reactivated again during subsequent, post-rift deformation of the cover rocks, it is evident the Selwyn Block basement faults influence structural geometry over multiple tectonic events, albeit at a large scale. The pervasive anisotropy of the Melbourne Zone may have exerted a greater control than the Selwyn Block faults on more closely-spaced fractures (i.e., Cretaceous rift-related normal faults). This example shows the importance of mapping structures in all of the basement units, at multiple scales, to explore the possibility of different wavelengths of basement influence.

Our findings demonstrate that in basins influenced by structural inheritance, fracture patterns are not scale-invariant. Therefore, a proper understanding of the structural architecture can only be achieved by analysing data that span multiple scales. This observation is relevant when we try to understand and predict the distribution and orientation of fractures, at regional, basin, and reservoir-scale, in order to model fluid transport in the crust. Our study also highlights the importance of mapping fractures in outcrop, which are analogous to naturally fractured reservoirs.

ACKNOWLEDGEMENTS

We thank Sam Thiele, Megan Withers, and Jonas Köpping for their assistance with data collection. Fieldwork was partly funded by an AAPG Grants-in-Aid Award awarded to AS. AS and SAV were supported by a Monash University Faculty of Science Dean's International Postgraduate Research Scholarship.

DATA AVAILABILITY

The basemap used for structural mapping at Shark Stack (Cape Liptrap) is available at 10 cm resolution from https://doi.org/10.26180/5c653193efa25 (Vollgger and Cruden, 2019). The datasets used for fracture mapping at Harmers Haven North, Harmers Haven South, Eagles Nest, the Caves–Flat Rocks, and Inverloch are available from https://monash.figshare.com/s/8063e7c3aaafaab24b83 (Samsu and Cruden, 2019).

REFERENCES

Aghaei, H., Hall, M., Wagstaff, B., and Tait, A., 2017, Stratigraphic reconstruction of the Strzelecki Group outcrops in west Gippsland: new data on the present-day thickness and amount of erosion: Australian Journal of Earth Sciences, v. 64, p. 251–264, doi:10.1080/08120099.2016.1278033.

570 Bourne, S.J., and Willemse, E.J.M., 2001, Elastic stress control on the pattern of tensile
571 fracturing around a small fault network at Nash Point, UK: Journal of Structural
572 Geology, v. 23, p. 1753–1770, doi:https://doi.org/10.1016/S0191-8141(01)00027-X.

573 Cayley, R.A., 2011, Exotic crustal block accretion to the eastern Gondwanaland margin in the
574 Late Cambrian-Tasmania, the Selwyn Block, and implications for the Cambrian-Silurian
575 evolution of the Ross, Delamerian, and Lachlan orogens: Gondwana Research, v. 19, p.
576 628–649, doi:10.1016/j.gr.2010.11.013.

577 Cayley, R.A., Taylor, D.H., VandenBerg, A.H.M., and Moore, D.H., 2002, Proterozoic -
578 Early Palaeozoic rocks and the Tyennan Orogeny in central Victoria: The Selwyn Block
579 and its tectonic implications: Australian Journal of Earth Sciences, v. 49, p. 225–254,
580 doi:10.1046/j.1440-0952.2002.00921.x.

581 Chantraprasert, S., McClay, K.R., and Elders, C., 2001, 3D Rift Fault Systems of the Western
582 Otway Basin, SE Australia, *in* Hill, K.C. and Bernecker, T. eds., Eastern Australasian
583 Basins Symposium, p. 435–446.

584 Cobbold, P.R., Cosgrove, J.W., and Summers, J.M., 1971, Development of internal structures
585 in deformed anisotropic rocks: Tectonophysics, v. 12, p. 23–53, doi:10.1016/0040-
586 1951(71)90065-5.

587 Collanega, L., Jackson, C.A., Bell, R.E., Coleman, A.J., Lenhart, A., and Breda, A., 2019,
588 Normal fault growth influenced by basement fabrics: the importance of preferential
589 nucleation from pre-existing structures: Basin Research, v. in press,
590 doi:10.1111/bre.12327.

591 Constantine, A., 2001, Sedimentology, Stratigraphy and Palaeoenvironment of the Upper
592 Jurassic-Lower Cretaceous Non-Marine Strzelecki Group, Gippsland Basin,
593 Southeastern Australia: Monash University. PhD Thesis.

Corti, G., van Wijk, J., Cloetingh, S., and Morley, C.K., 2007, Tectonic inheritance and continental rift architecture: Numerical and analogue models of the East African Rift system: Tectonics, v. 26, p. 1–13, doi:10.1029/2006TC002086.

Cruikshank, K.M., and Aydin, A., 1995, Unweaving the joints in Entrada Sandstone, Arches National Park, Utah, U.S.A.: Journal of Structural Geology, v. 17, p. 409–421, doi:10.1016/0191-8141(94)00061-4.

Dering, G.M., Micklethwaite, S., Thiele, S.T., Vollgger, S.A., and Cruden, A.R., 2019, Review of drones, photogrammetry and emerging sensor technology for the study of dykes: Best practises and future potential: Journal of Volcanology and Geothermal Research, doi:10.1016/j.jvolgeores.2019.01.018.

Duddy, I.R., and Green, P.F., 1992, Tectonic development of the Gippsland Basin and environs: identification of key episodes using Apatite Fission Track Analysis (AFTA), *in* Gippsland Basin Symposium 22-23 June 1992, Melbourne, p. 111–120.

Dumitru, T.A., Hill, K.C., Coyle, D.A., Duddy, I.R., Foster, D.A., Gleadow, A.J.W., Green, P.F., Kohn, B.P., Laslett, G.M., and O'Sullivan, P.B., 1991, Fission track thermochronology: Application to continental rifting of south-eastern Australia: The APEA Journal, v. 31, p. 131–142.

Etheridge, M.A., Branson, J.C., and Stuart-Smith, P.G., 1985, Extensional basin-forming structures in Bass Strait and their importance for hydrocarbon exploration: The APEA Journal, v. 25, p. 344–361.

Fazlikhani, H., Fossen, H., Gawthorpe, R.L., Faleide, J.I., and Bell, R.E., 2017, Basement structure and its influence on the structural configuration of the northern North Sea rift: Tectonics, v. 36, p. 1151–1177, doi:10.1002/2017TC004514.

617 Foster, D.A., and Gleadow, A.J.W., 1992, Reactivated tectonic boundaries and implications
618 for the reconstruction of southeastern Australia and northern Victoria Land, Antarctica:
619 Geology, v. 20, p. 267–270, doi:10.1130/0091-
620 7613(1992)020<0267:RTBAIF>2.3.CO;2.

621 Gardner, T., Webb, J., Pezzia, C., Amborn, T., Tunnell, R., Flanagan, S., Merritts, D.,
622 Marshall, J., Fabel, D., and Cupper, M.L., 2009, Episodic intraplate deformation of
623 stable continental margins: evidence from Late Neogene and Quaternary marine
624 terraces, Cape Liptrap, Southeastern Australia: Quaternary Science Reviews, v. 28, p.
625 39–53, doi:10.1016/j.quascirev.2008.10.004.

626 Gray, D.R., Janssen, C., and Vapnik, Y., 1999, Deformation character and palaeo-fluid flow
627 across a wrench fault within a Palaeozoic subduction-accretion system: Waratah Fault
628 Zone, southeastern Australia: Journal of Structural Geology, v. 21, p. 191–214,
629 doi:10.1016/S0191-8141(98)00115-1.

630 Gray, D.R., and Mortimer, L., 1996, Implications of overprinting deformations and fold
631 interference patterns in the Melbourne Zone, Lachlan Fold Belt: Australian Journal of
632 Earth Sciences, v. 43, p. 103–114, doi:10.1080/08120099608728240.

633 Healy, D., Rizzo, R.E., Cornwell, D.G., Farrell, N.J.C., Watkins, H., Timms, N.E., Gomez-
634 Rivas, E., and Smith, M., 2016, FracPaQ: A MATLAB^{TM} toolbox for the quantification
635 of fracture patterns: Journal of Structural Geology, v. 95, p. 1–16,
636 doi:10.1016/j.jsg.2016.12.003.

637 Heilman, E., Kolawole, F., Atekwana, E.A., and Mayle, M., 2019, Controls of Basement
638 Fabric on the Linkage of Rift Segments: Tectonics, doi:10.1029/2018TC005362.

639 Henza, A.A., Withjack, M.O., and Schlische, R.W., 2011, How do the properties of a pre-
640 existing normal-fault population influence fault development during a subsequent phase

641 of extension? Journal of Structural Geology, v. 33, p. 1312–1324,
642 doi:10.1016/j.jsg.2011.06.010.

643 Hill, K.A., Cooper, G.T., Richardson, M.J., and Lavin, C.J., 1994, Structural framework of
644 the Eastern Otway basin: inversion and interaction between two major structural
645 provinces: Exploration Geophysics, v. 25, p. 79–87, doi:10.1071/EG994079.

646 Hill, K.C., Hill, K.A., Cooper, G.T., O'Sullivan, A.J., O'Sullivan, P.B., and Richardson, M.J.,
647 1995, Inversion around the Bass Basin, SE Australia: Geological Society, London,
648 Special Publications, v. 88, p. 525–547, doi:10.1144/GSL.SP.1995.088.01.27.

649 Hillis, R.R., and Reynolds, S.D., 2000, The Australian Stress Map: Journal of the Geological
650 Society, v. 157, p. 915–921, doi:10.1144/jgs.157.5.915.

651 Holdgate, G.R., Rodriquez, C., Johnstone, E.M., Wallace, M.W., and Gallagher, S.J., 2003,
652 The Gippsland Basin Top Latrobe Unconformity and its expression in other Southeast
653 Australia basins: The APPEA Journal, v. 43, p. 149–173.

654 Holdsworth, R.E., Butler, C.A., and Roberts, A.M., 1997, The recognition of reactivation
655 during continental deformation: Journal of the Geological Society, v. 154, p. 73–78,
656 doi:10.1144/gsjgs.154.1.0073.

657 de Joussineau, G., Petit, J.P., and Gauthier, B.D.M., 2003, Photoelastic and numerical
658 investigation of stress distributions around fault models under biaxial compressive
659 loading conditions: Tectonophysics, v. 363, p. 19–43, doi:10.1016/S0040-
660 1951(02)00648-0.

661 Kapp, M.W., Hohenwarter, A., Wurster, S., Yang, B., and Pippan, R., 2016, Anisotropic
662 deformation characteristics of an ultrafine- and nanolamellar pearlitic steel: Acta
663 Materialia, v. 106, p. 239–248, doi:10.1016/j.actamat.2015.12.037.

Keetley, J.T., Hill, K.C., and Nguyen, C., 2001, Mesoscopic fold and thrust structures at Cape Liptrap, Victoria, Australia; a PNG analogue?, *in* Hill, K.C. and Bernecker, T. eds., Eastern Australasian Basins Symposium, p. 25–28.

Kirkpatrick, J.D., Bezerra, F.H.R., Shipton, Z.K., Do Nascimento, A.F., Pytharouli, S.I., Lunn, R.J., and Soden, A.M., 2013, Scale-dependent influence of pre-existing basement shear zones on rift faulting: a case study from NE Brazil: Journal of the Geological Society, v. 170, p. 237–247, doi:10.1144/jgs2012-043.

Krassay, A.A., Cathro, D.L., and Ryan, D.J., 2004, A regional tectonostratigraphic framework for the Otway Basin: Eastern Australasian Basins Symposium II, p. 97–116.

Lavenu, A.P.C., Lamarche, J., Gallois, A., and Gauthier, B.D.M., 2013, Tectonic versus diagenetic origin of fractures in a naturally fractured carbonate reservoir analog (Nerthe anticline, southeastern France): AAPG Bulletin, v. 97, p. 2207–2232, doi:10.1306/04041312225.

Maerten, L., Gillespie, P., and Pollard, D.D., 2002, Effects of local stress perturbation on secondary fault development: Journal of Structural Geology, v. 24, p. 145–153, doi:10.1016/S0191-8141(01)00054-2.

Marchegiani, L., Van Dijk, J.P., Gillespie, P. a, Tondi, E., and Cello, G., 2006, Scaling properties of the dimensional and spatial characteristics of fault and fracture systems in the Majella Mountain, central Italy: Geological Society Special Publication, v. 261, p. 113–131, doi:10.1144/GSL.SP.2006.261.01.09.

McLean, M.A., Morand, V.J., and Cayley, R.A., 2010, Gravity and magnetic modelling of crustal structure in central Victoria: what lies under the Melbourne Zone? Australian Journal of Earth Sciences, v. 57, p. 153–173, doi:10.1080/08120090903416245.

687 Miller, J.M.L., Norvick, M.S., and Wilson, C.J.L., 2002, Basement controls on rifting and the
688 associated formation of ocean transform faults - Cretaceous continental extension of the
689 southern margin of Australia: Tectonophysics, v. 359, p. 131–155, doi:10.1016/S0040-
690 1951(02)00508-5.

691 Moore, D.H., Betts, P.G., and Hall, M., 2016, Constraining the VanDieland microcontinent at
692 the edge of East Gondwana, Australia: Tectonophysics, v. 687, p. 158–179,
693 doi:10.1016/j.tecto.2016.09.009.

694 Morley, C.K., 2010, Stress re-orientation along zones of weak fabrics in rifts: An explanation
695 for pure extension in “oblique” rift segments? Earth and Planetary Science Letters, v.
696 297, p. 667–673, doi:10.1016/j.epsl.2010.07.022.

697 Morley, C.K., Nelson, R.A., Patton, T.L., and Munn, S.G., 1990, Transfer zones in the East
698 African rift system and their relevance to hydrocarbon exploration in rifts: AAPG
699 Bulletin, v. 74, p. 1234–1253, doi:10.1306/0C9B2475-1710-11D7-8645000102C1865D.

700 Munro, M.A., and Blenkinsop, T.G., 2012, MARD-A moving average rose diagram
701 application for the geosciences: Computers and Geosciences, v. 49, p. 112–120,
702 doi:10.1016/j.cageo.2012.07.012.

703 Norvick, M.S., and Smith, M.S., 2001, Mapping the plate tectonic reconstruction of southern
704 and southeastern Australia and implications for petroleum systems: The APPEA Journal,
705 v. 41, p. 15–35.

706 Norvick, M.S., Smith, M.A., and Power, M.R., 2001, The Plate Tectonic Evolution of Eastern
707 Australasia Guided by the Stratigraphy of the Gippsland Basin, *in* Eastern Australasian
708 Basins Symposium, Hill, K.C. Bernecker, T., p. 15–23.

709 Peace, A., McCaffrey, K., Imber, J., van Hunen, J., Hobbs, R., and Wilson, R., 2018, The role

of pre-existing structures during rifting, continental breakup and transform system development, offshore West Greenland: Basin Research, v. 30, p. 373–394, doi:10.1111/bre.12257.

Phillips, T.B., Jackson, C.A.L., Bell, R.E., Duffy, O.B., and Fossen, H., 2016, Reactivation of intrabasement structures during rifting: A case study from offshore southern Norway: Journal of Structural Geology, v. 91, p. 54–73, doi:10.1016/j.jsg.2016.08.008.

Power, M.R., Hill, K.C., and Hoffman, N., 2003, Structural inheritance, stress rotation, overprinting and compressional reactivation in the Gippsland Basin - Tuna 3D seismic dataset: The APPEA Journal, v. 43, p. 197–221, doi:https://doi.org/10.1071/AJ02010.

QGIS Development Team, 2019, QGIS Geographic Information System. Open Source Geospatial Foundation Project.:

Reeve, M.T., Bell, R.E., Duffy, O.B., Jackson, C.A.L., and Sansom, E., 2015, The growth of non-colinear normal fault systems; What can we learn from 3D seismic reflection data? Journal of Structural Geology, v. 70, p. 141–155, doi:10.1016/j.jsg.2014.11.007.

Robin, P.Y.F., and Jowett, E.C., 1986, Computerized density contouring and statistical evaluation of orientation data using counting circles and continuous weighting functions: Tectonophysics, v. 121, p. 207–223, doi:10.1016/0040-1951(86)90044-2.

Rohrbaugh, M.B.J., Dunne, W.M., and Mauldon, M., 2002, Estimating fracture trace intensity, density, and mean length using circular scan lines and windows: AAPG Bulletin, v. 86, p. 2089–2104, doi:10.1306/61EEDE0E-173E-11D7-8645000102C1865D.

Samsu, A., Cruden, A.R., Hall, M., Micklethwaite, S., and Denyszyn, S.W., 2019, The influence of basement faults on local extension directions: Insights from potential field

733 geophysics and field observations: Basin Research, v. 00, p. 1–26,
734 doi:10.1111/bre.12344.

735 Stubley, M.P., 1989, Fault and kink-band relationships at Mystery Bay, Australia:
736 Tectonophysics, v. 158, p. 75–92, doi:10.1016/0040-1951(89)90317-X.

737 Teasdale, J.P. et al., 2004, Australian Southern Margin SEEBASE™ Compilation, April
738 2004:, https://data.gov.au/dataset/9131aad8-7d83-4a2b-a678-542e2a1af68a (accessed
739 June 2018).

740 Thiele, S.T., Grose, L., Samsu, A., Micklethwaite, S., Vollgger, S.A., and Cruden, A.R.,
741 2017, Rapid, semi-automatic fracture and contact mapping for point clouds, images and
742 geophysical data: Solid Earth, v. 8, p. 1241–1253, doi:10.5194/se-8-1241-2017.

743 Tveite, H., 2015, The QGIS Line Direction Histogram Plugin:,
744 http://arken.nmbu.no/~havatv/gis/qgisplugins/LineDirectionHistogram/ (accessed July
745 2016).

746 VandenBerg, A.H.M. et al., 2006, Walhalla–Woods Point–Tallangallook special map area
747 geological report: GeoScience Victoria. Department of Primary Industries.

748 VandenBerg, A.H.M., Willman, C.E., Maher, S., Simons, B.A., Cayley, R.A., Taylor, D.H.,
749 Morand, V.J., Moore, D.H., and Radojkovic, A., 2000, The Tasman Fold Belt System in
750 Victoria: Geological Survey of Victoria Special Publication, p. 462.

751 Vollgger, S., and Cruden, A., 2019, Cape Liptrap orthomosaic:,
752 doi:https://doi.org/10.26180/5c653193efa25.

753 Vollgger, S.A., and Cruden, A.R., 2016, Mapping folds and fractures in basement and cover
754 rocks using UAV photogrammetry, Cape Liptrap and Cape Paterson, Victoria, Australia:
755 Journal of Structural Geology, v. 85, p. 168–187, doi:10.1016/j.jsg.2016.02.012.

Watkins, H., Bond, C.E., Healy, D., and Butler, R.W.H., 2015, Appraisal of fracture sampling methods and a new workflow to characterise heterogeneous fracture networks at outcrop: Journal of Structural Geology, v. 72, p. 67–82, doi:10.1016/j.jsg.2015.02.001.

Welch, M.J., Souque, C., Davies, R.K., and Knipe, R.J., 2014, Using mechanical models to investigate the controls on fracture geometry and distribution in chalk: Geological Society, London, Special Publications, v. 406, p. 281–309, doi:10.1144/sp406.5.

Whipp, P.S., Jackson, C.A.L., Gawthorpe, R.L., Dreyer, T., and Quinn, D., 2014, Normal fault array evolution above a reactivated rift fabric; a subsurface example from the northern Horda Platform, Norwegian North Sea: Basin Research, v. 26, p. 523–549, doi:10.1111/bre.12050.

Willcox, J.B., Colwell, J.B., and Constantine, A.E., 1992, New ideas on Gippsland Basin regional tectonics, *in* Gippsland Basin Symposium 22-23 June 1992, Melbourne, p. 93–110.

Wilson, R.W., Holdsworth, R.E., Wild, L.E., McCaffrey, K.J.W., England, R.W., Imber, J., and Strachan, R.A., 2010, Basement-influenced rifting and basin development: a reappraisal of post-Caledonian faulting patterns from the North Coast Transfer Zone, Scotland: Geological Society, London, Special Publications, v. 335, p. 795–826, doi:10.1144/SP335.32.

Wilson, C.J.L., Moore, D.H., Luzin, V., and Salvemini, F., 2017, Costerfield antimony-gold deposit, southeast Australia: Coupling between brittle deformation and dissolution-precipitation reactions in the Melbourne Zone: Ore Geology Reviews, v. 91, p. 741–764, doi:10.1016/j.oregeorev.2017.08.024.

Wu, H., and D. Pollard, D., 1995, An experimental study of the relationship between joint

780 spacing and layer thickness: Journal of Structural Geology, v. 17, p. 887–905,
781 doi:10.1016/0191-8141(94)00099-L.

782

783 **Table 1** Summary of the sequence of ductile and brittle deformation at Shark Stack. The
784 orientation of the trace of the structure on aerial imagery, the sense of movement along the
785 horizontal, and the inferred orientation of the maximum horizontal principle stress (σ_H) are
786 included.

Event	Structures	Trace Azimuth		Sense of Movement	Regime	σ_H Orientation
D1	F1 folds	NNE-SSW	3 - 37°		Contraction	WNW-ESE
D2	F2 folds	N-S	355 - 15°	Dextral	Contraction	NNE-SSW
D3	Fractures	ENE-WSW	50 - 75°	Dextral	Extension	ENE-WSW
D4	F4 kinks	NW-SE	310 - 320°	Dextral	Contraction	NNW-SSE
D4	Fractures	NNW-SSE	315 - 360°	Sinistral	Contraction	NNW-SSE

787

788 **Table 2** Fracture trends in Lower Cretaceous Strzelecki Group outcrops. $N_{L\leq 50m}$ = total
789 number of fracture traces at each locality with a length ≤ 50 m; N_{Trend} = number of fracture
790 traces belonging to the corresponding trend.

Locality	**$N_{L\leq 50m}$**	**Trend Azimuth**		**N_{Trend}**
Harmers Haven North	1308	NNW-SSE	335 - 350°	267
		WNW-ESE	280 - 295°	246
		E-W	80 - 100°	259
Harmers Haven South	2497	NNW-SSE	325 - 345°	1055
Eagles Nest	1443	NNW-SSE	325 - 345°	404
		ENE-WSW	65 - 80°	180
		E-W	80 - 95°	188
The Caves - Flat Rocks	1591	NNW-SSE	320 - 345°	522
		ENE-WSW	65 - 85°	239
		NNE-SSW	10 - 20°	126
Inverloch	378	NW-SE to NNW-SSE	315 - 345°	141
		E-W	85 - 90°	27
		WNW-ESE to NW-SE	290 - 315°	86

791

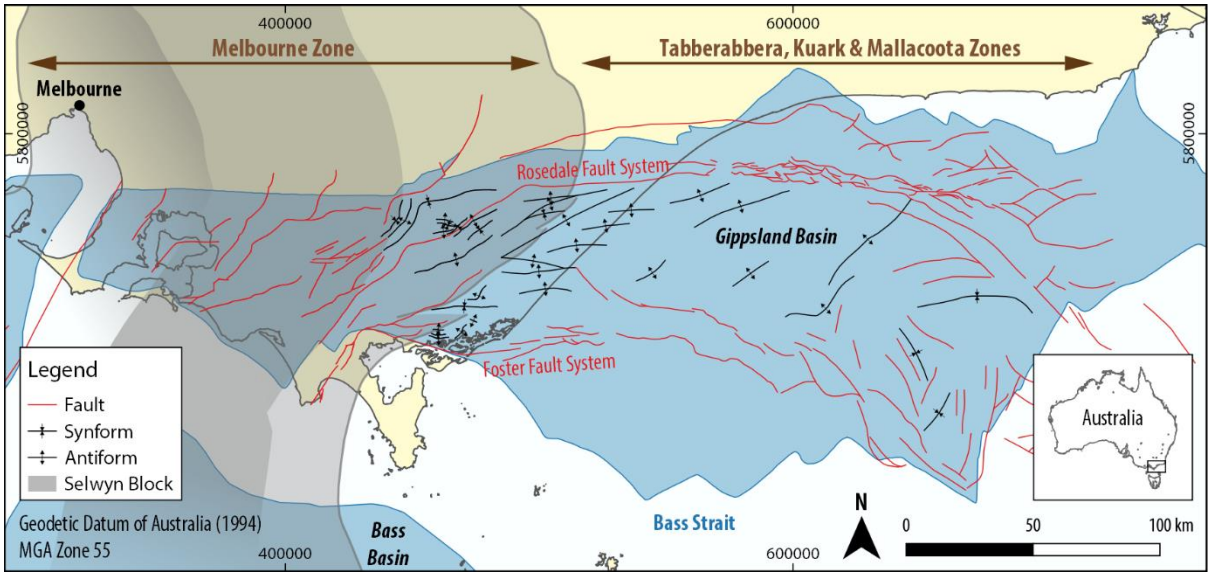

Figure 1 Location and major structures of the Cretaceous Gippsland Basin and the nearby Bass Basin (shaded in blue). Areas that are underlain by the Selwyn Block (Moore et al., 2016) and Melbourne Zone are shaded in grey. Faults and folds in the Gippsland Basin are modified after Constantine (2001) and Power et al. (2001). From west to east, structural trends change from NE-SW and ENE-WSW (western onshore Gippsland Basin), to E-W and NW-SE (eastern onshore and offshore Gippsland Basin); this transition coincides spatially with the eastern margin of the Selwyn Block. The coordinate reference system is GDA94 / MGA zone 55.

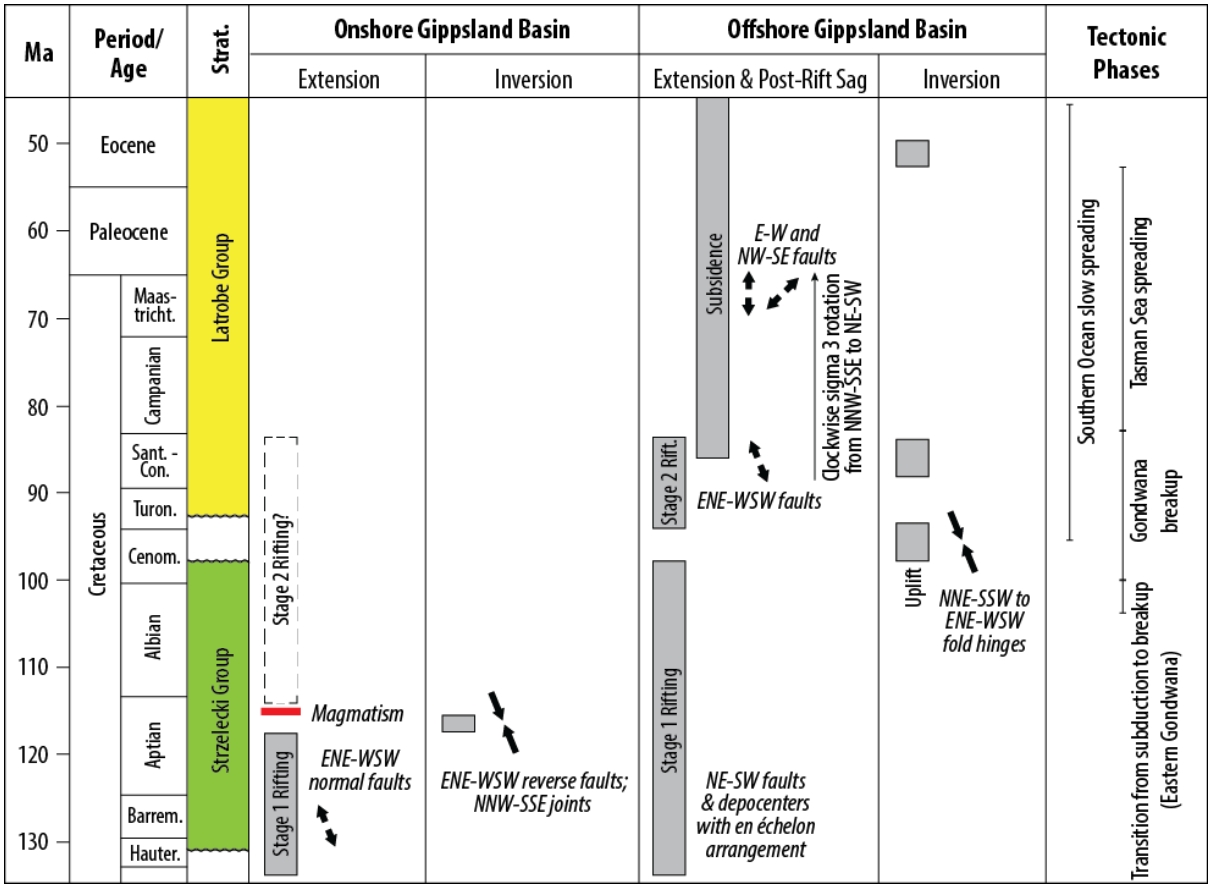

Figure 2 Summary of the deformation history in the Gippsland Basin and associated tectonic events. Deformation events in the offshore Gippsland Basin are derived from seismic reflection studies (Power et al., 2003). Cretaceous deformation in the onshore Gippsland Basin is derived from field studies and regional potential field geophysics (Samsu et al., 2019).

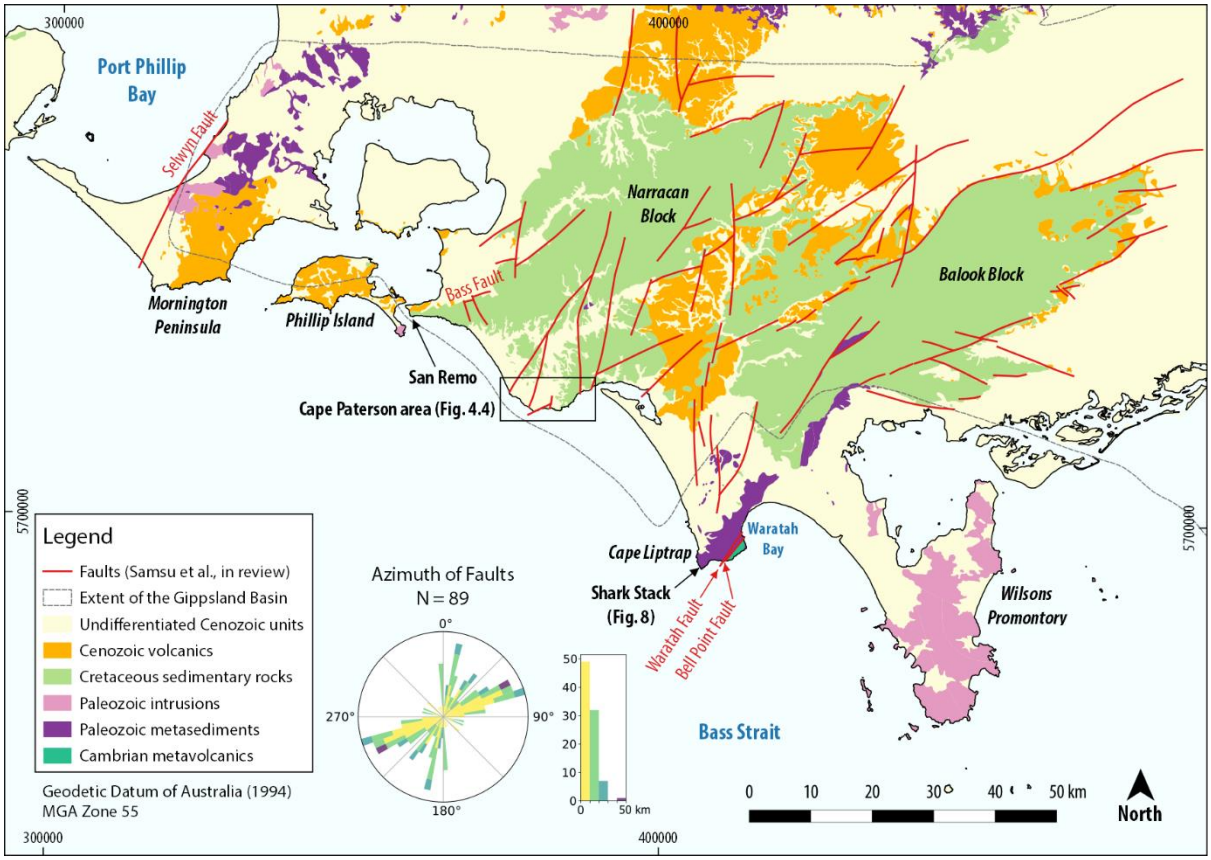

Figure 3 Map of basin-scale (>1 km-scale) faults interpreted from magnetic and gravity data (modified after Samsu et al., 2019). The rose diagram of fault traces was created using the GeoTrace plugin (Thiele et al., 2017) in QGIS and is coloured by fault length. Colours on the rose diagram correlate with fault length bins shown on the length histogram. The coordinate reference system is GDA94 / MGA zone 55.

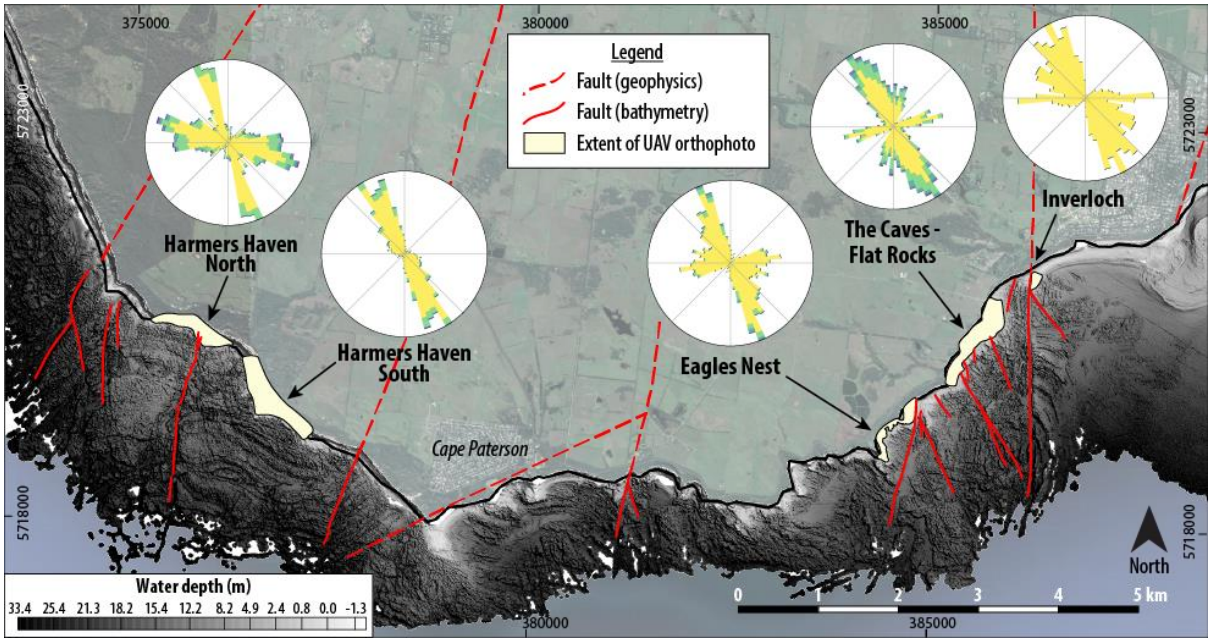

Figure 4 Map of the UAV photogrammetry survey areas, where outcrop-scale fractures in the Lower Cretaceous Strzelecki Group were traced, overlain on a greyscale image of near-shore bathymetry (modified after Samsu et al., 2019). The frequency of the orientations of fracture traces from each area is visualized as length-coloured rose diagrams. Colours correspond to fracture length, subdivided into 10 m bins (see Fig. 5 for colour ramp of length bins). See Fig. 3 for location of map.

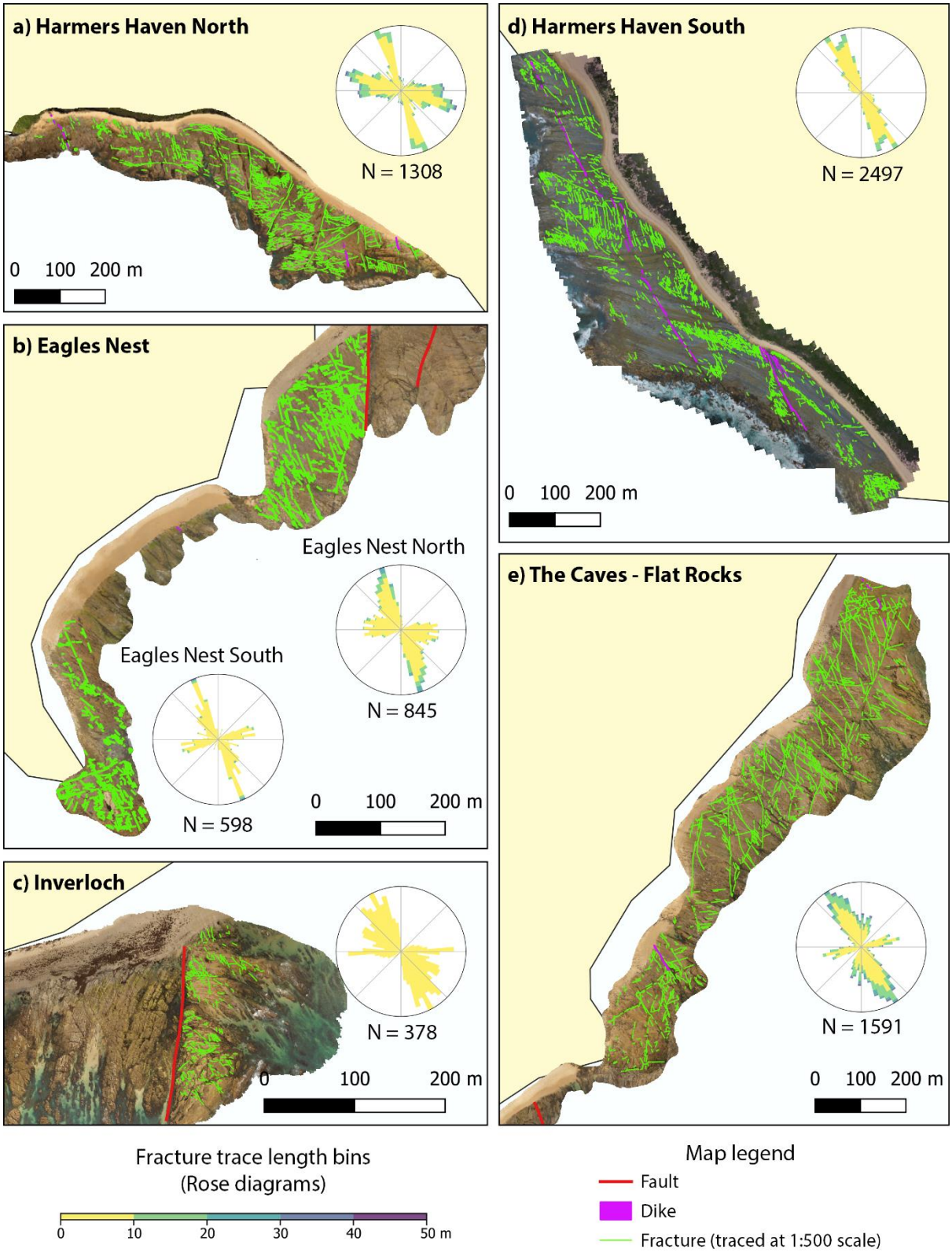

820

821 **Figure 5** Fracture trace maps and rose diagrams, representing fractures <50 m in length, for
822 the five studied outcrops (see Fig. 4 for locations). Fracture traces (interpreted at a scale of
823 1:500) are overlain on UAV orthophotos. Colours on the rose diagram correspond to fracture
824 length, subdivided into 10 m bins.

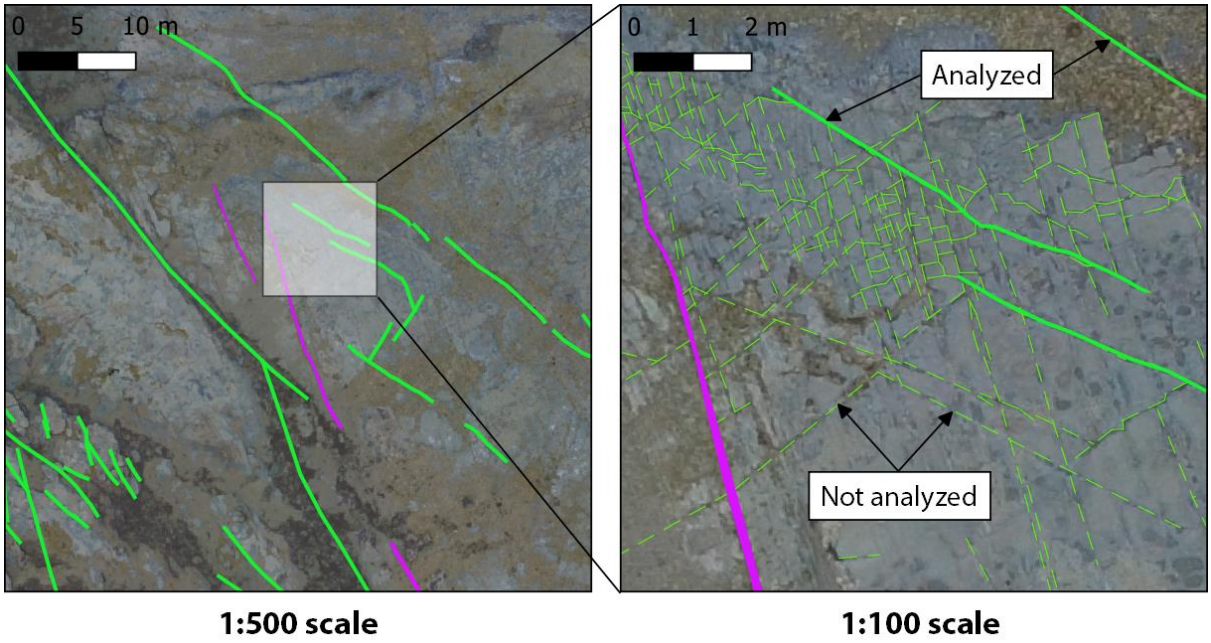

825

826 **Figure 6** Fracture traces (green) interpreted from UAV orthophotos at 1:500 and 1:100 zoom
827 levels. Fractures that can be seen at the 1:500 scale (thick, continuous lines) were included in
828 the analyses of fracture orientations, so that we only compare fractures between outcrops that
829 are observable at the same scale. Purple traces represent mafic dikes.

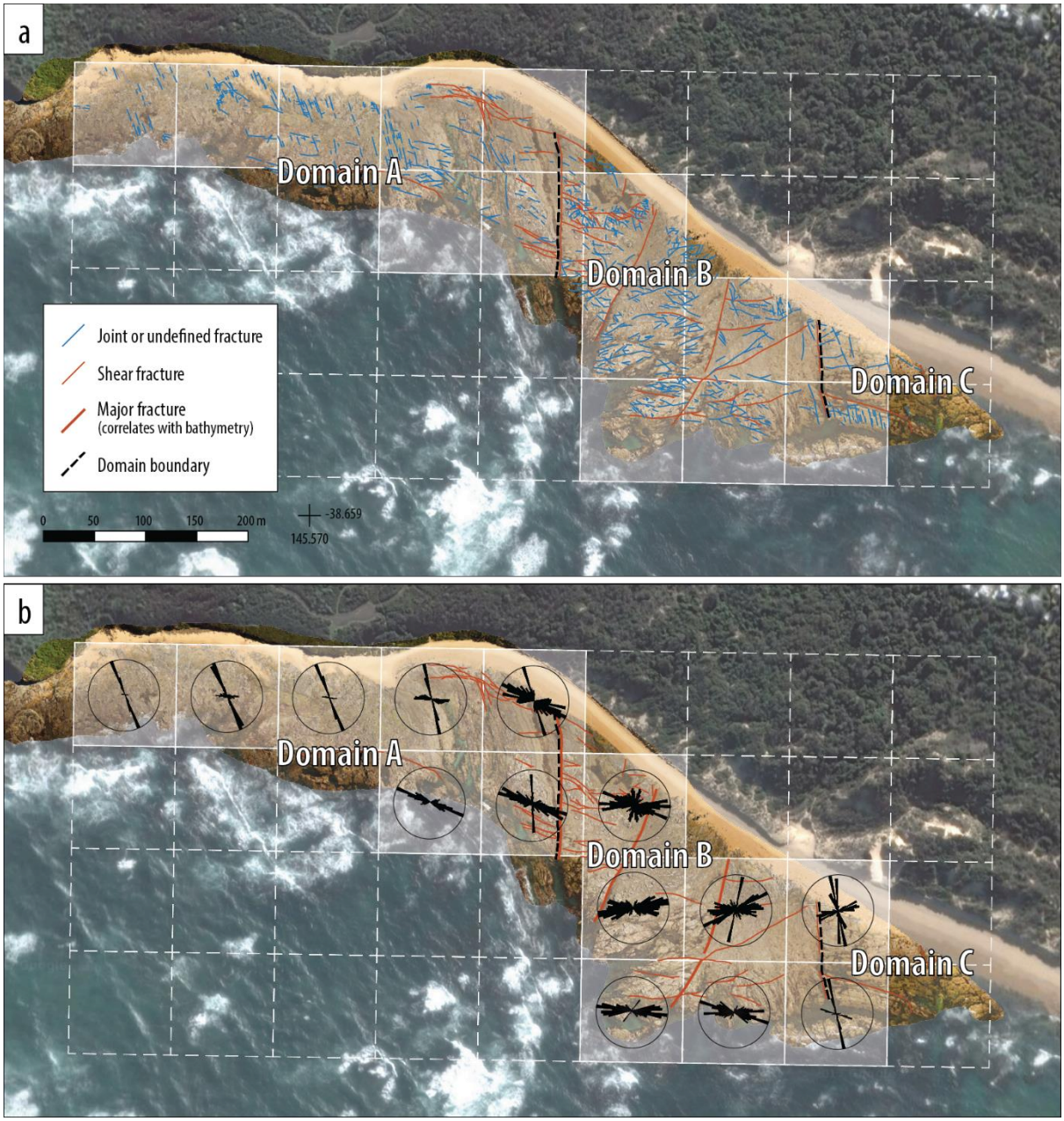

Figure 7 (a) Fracture trace map of the Harmers Haven North locality. The basemap is a high-resolution (3 cm/pixel) UAV orthophoto. A grid made up of 100 m x 100 m tiles is overlain on the orthophoto. (b) Length-weighted rose diagrams of fracture trace orientations calculated for each tile using the Line Direction Histogram plugin (Tveite, 2015) in QGIS. The background is a satellite image (source: Google Earth, 38.657362° and 145.572051°, May 14, 2016, accessed July 30, 2017).

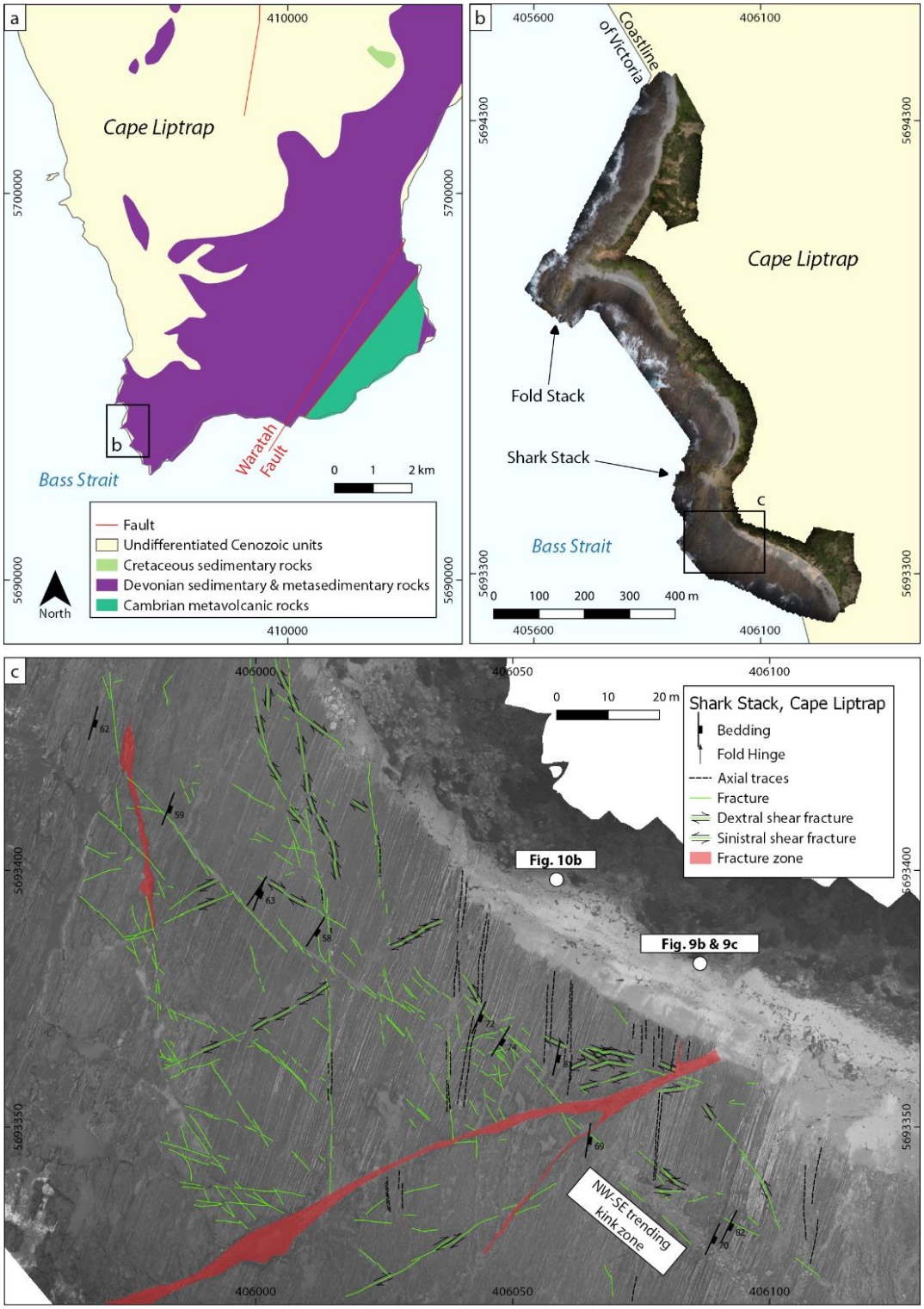

Figure 8 (a) Location of Shark Stack study area at the southwestern end of Cape Liptrap (see Fig. 3 for location), where a UAV orthophoto (b; 2 cm/pixel) was used as a basemap for structural mapping in the field. Structures at the Fold Stack locality have been described in detail in Vollgger and Cruden (2016). (c) Map of fractures, axial traces of folds, and structural measurements at Shark Stack. All of the fractures that are visible at a 1:500 scale are shown.

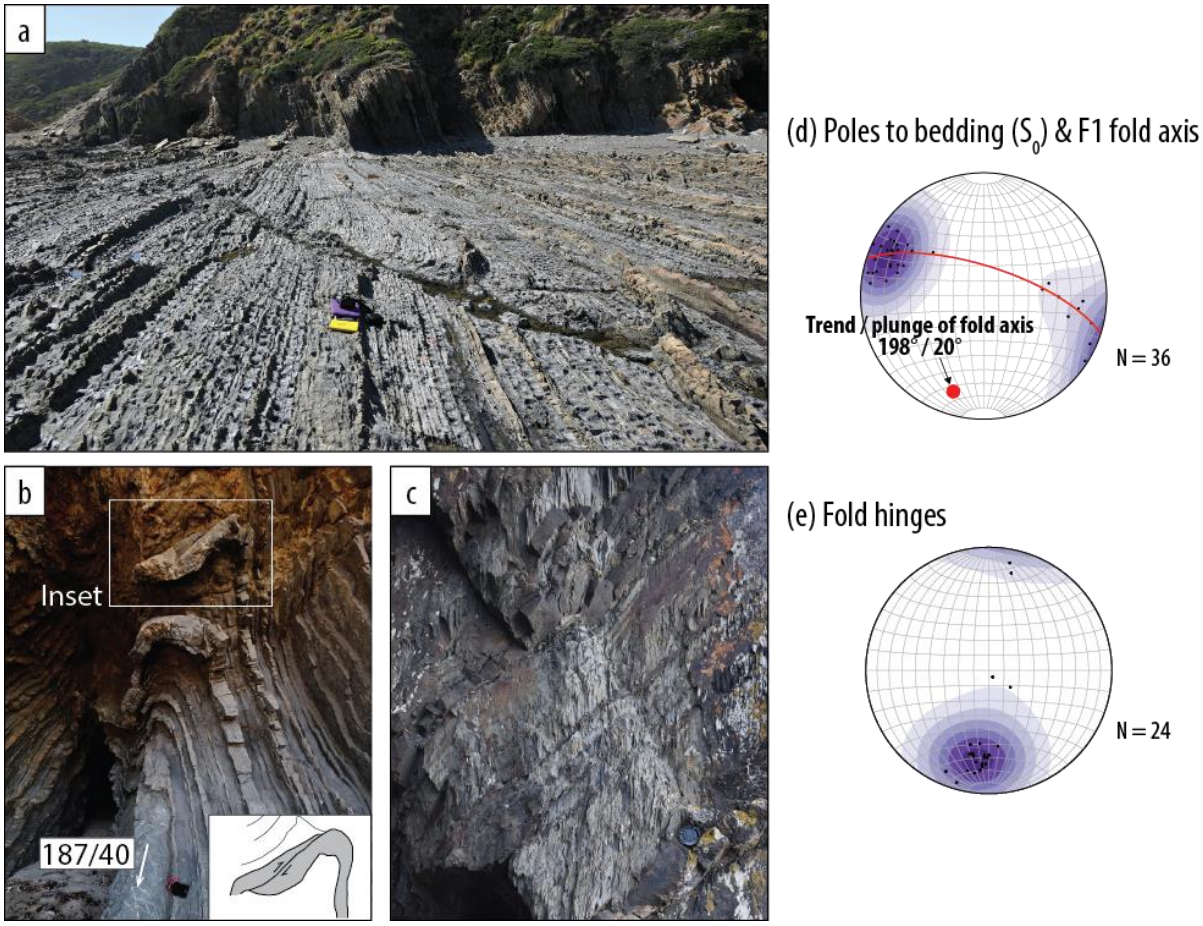

Figure 9 Structures at Shark Stack, Cape Liptrap: (a) Photograph of steeply dipping, alternating beds of sandstone and mudstone cropping out on a horizontal wavecut platform and along vertical cliff faces. These rocks form the Devonian basement underlying the onshore Gippsland Basin. (b) Photograph of disharmonic second-order F2 folds exposed in a cliff face. The inset shows a fold accommodation fault offsetting a sandstone bed in a reverse sense near the fold hinge. The arrow indicates the measured orientation of the hinge line. (c) Photograph of axial planar cleavage and parasitic folds on the limb of an F1 fold. (d) Plot of poles to bedding measurements and the axis of a first-order F1 fold calculated from bedding measurements. The calculated fold axis is consistent with the orientation of the measured axial planar cleavage, which is orthogonal to the fold axis. (e) Plot of measured fold hinges; shallowly plunging fold hinges are F2 fold hinges associated with a D2 contractional event. Pole orientations were contoured using the Exponential Kamb method at intervals of 3σ.

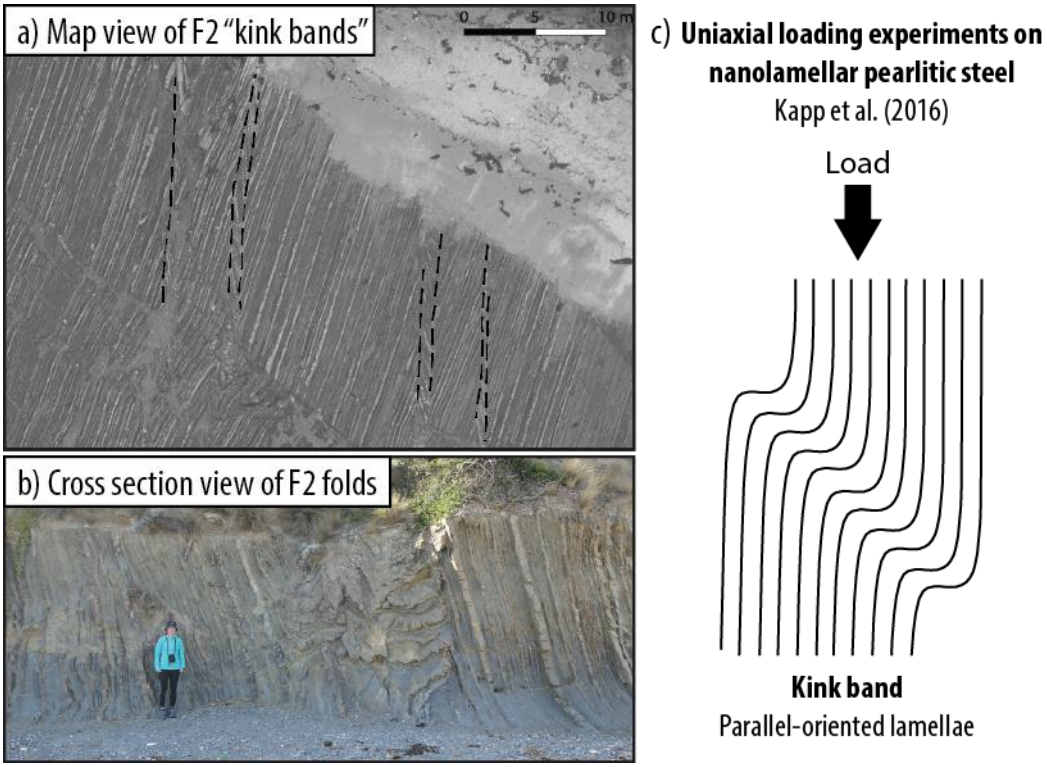

857

858 **Figure 10** N-S trending zones of kinking in the wavecut platform (a) and cliff (b). Dashed
859 lines represent axial traces of F2 kink bands. Kink bands at Shark Stack are analogous to kink
860 bands in nanolamellar pearlitic steel (c) (modified after Kapp et al., 2016).

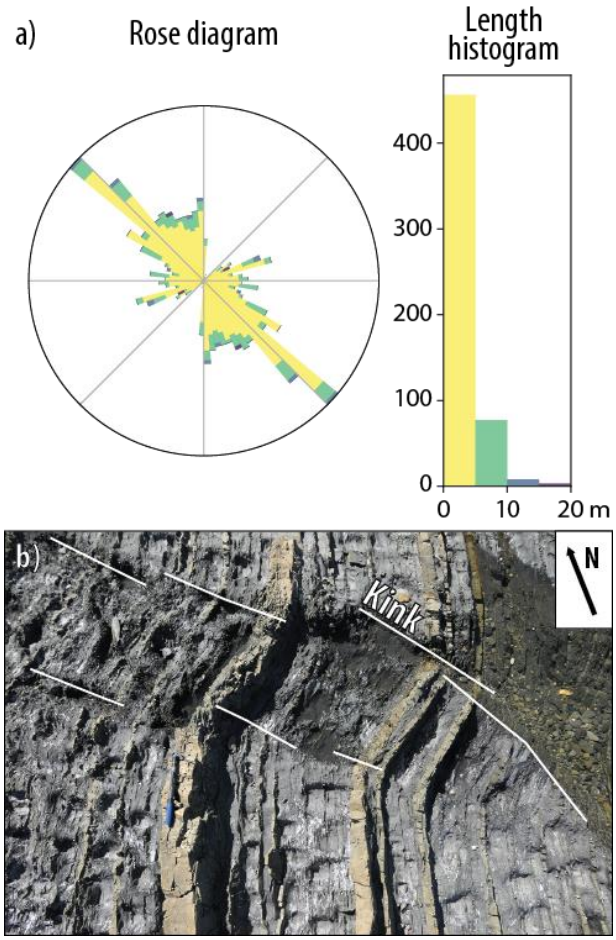

Figure 11 (a) Length-coloured rose diagram of outcrop-scale fractures at Shark Stack. (b) The NW-SE trending peak represents a large population of kinks that make up the NW-SE trending F3 kink bands. The length-coloured rose diagram allows us to assign fractures of different length ranges to certain orientation trends. NW-SE kinks are <10 m in length, most of them being shorter than 5 m. Fractures that are longer than 10 m trend NNW-SSE and ENE-WSW.

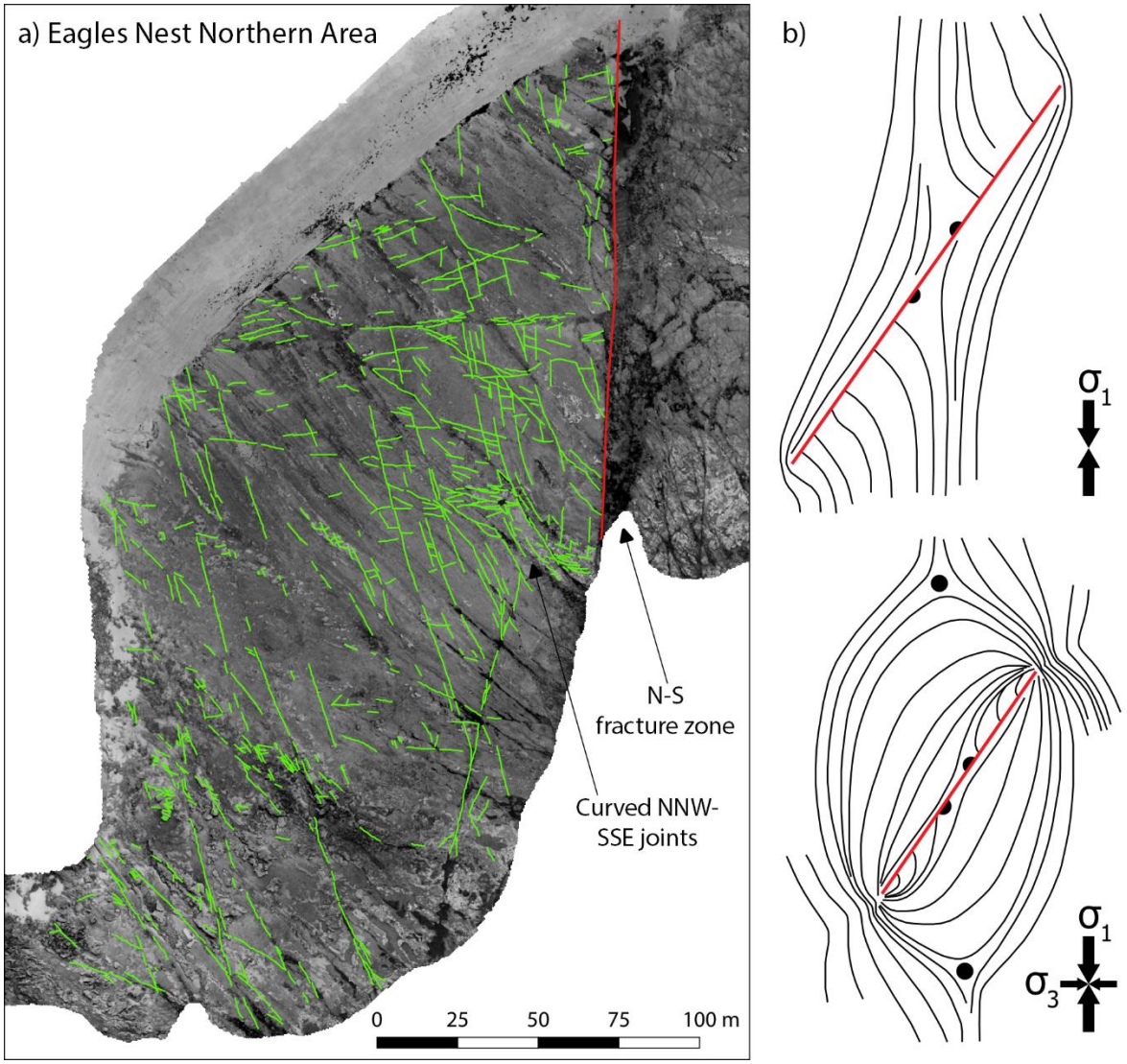

868

869 **Figure 12** (a) Fracture traces at the northern part of the Eagles Nest locality, overlain on a
870 high-resolution (3.2 cm/pixel) UAV orthophoto (See Fig. 4 for location). Veering of NNW-
871 SSE trending joints in the vicinity of the large N-S trending fault is observed, which may be
872 caused by perturbed stress trajectories around the larger fault. A similar phenomenon has
873 been observed in photoelastic experiments of uniaxial and biaxial loading on analogue
874 materials (b; modified from de Joussineau et al., 2003). The red line represents a pre-existing
875 fault, and black circles and half circles are isotropic points.

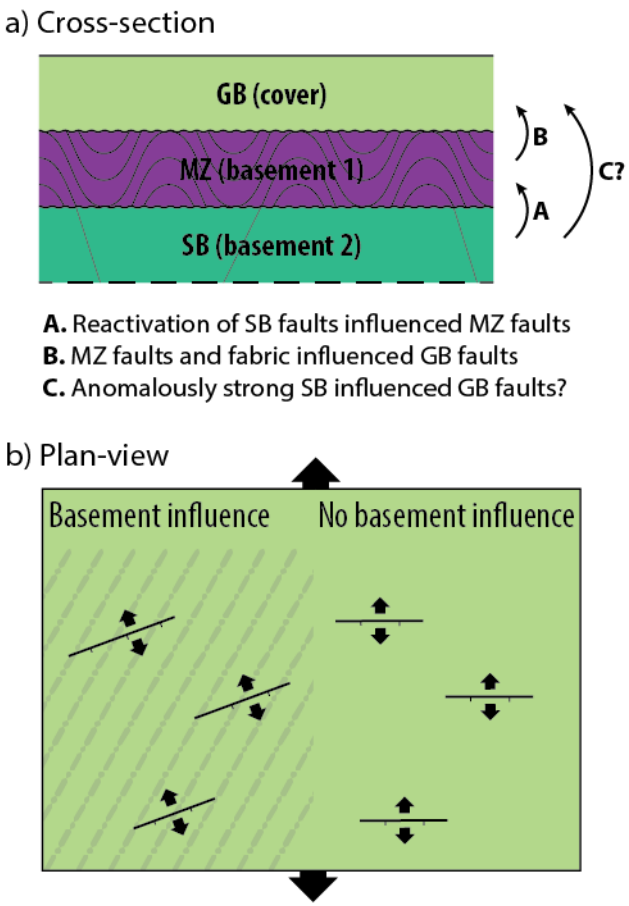

876

877 **Figure 13** (a) Schematic cross section demonstrating the influence of different basement
878 units on overlying units. Devonian faulting in the Melbourne Zone could have been
879 controlled by the reactivation of pre-existing Cambrian faults in the Selwyn Block (A). The
880 complex array of Early Cretaceous normal faults could have resulted from local stress re-
881 orientation above Devonian faults and penetrative fabrics in the Melbourne Zone (B). It
882 remains unclear how the relatively high strength of the Selwyn Block, juxtaposed against the
883 weaker surrounding lower crust, could have affected Early Cretaceous rifting (C). GB =
884 Gippsland Basin; MZ = Melbourne Zone; SB = Selwyn Block. (b) Schematic map-view
885 illustration of normal fault orientations: They are oblique to the regional extension direction
886 above an anisotropic basement, but they are orthogonal to regional extension where the
887 basement is less influential.

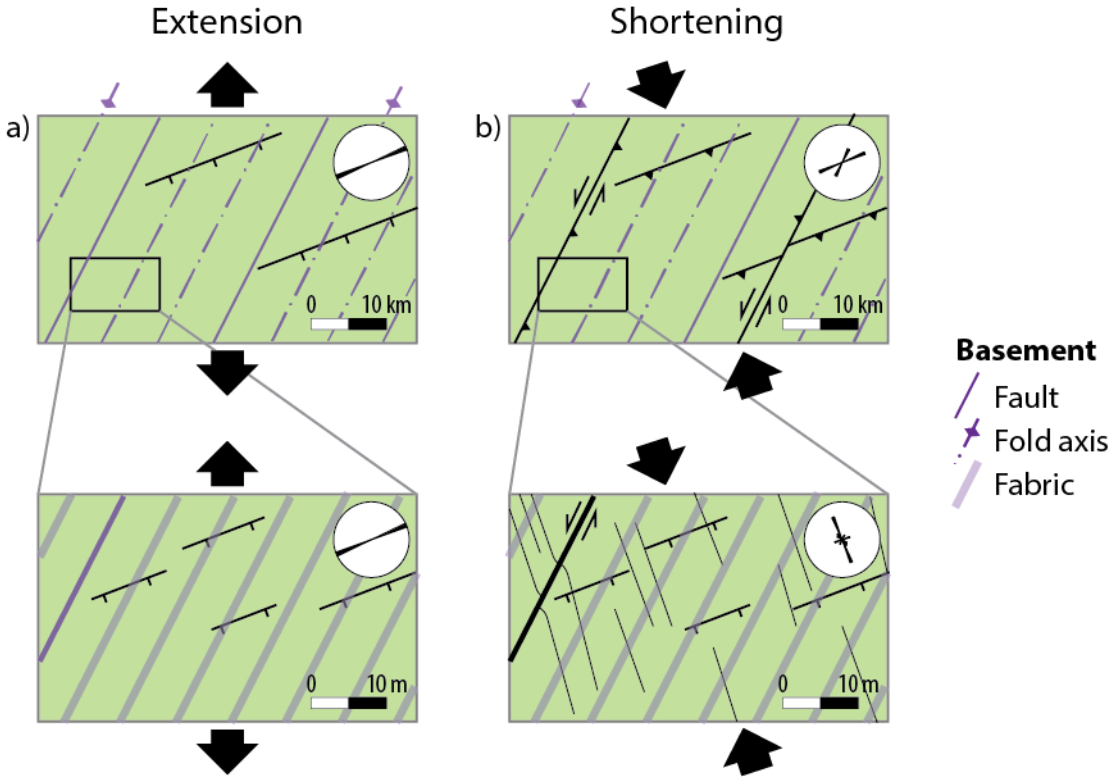

888

889 **Figure 14** Plan-view schematic illustration of fracture traces in the cover – associated with
890 Early Cretaceous extension (a) followed by shortening (b) – and their trends. The purple lines
891 represent structures in the underlying Melbourne Zone basement. Extension-related fractures
892 show the same ENE-WSW trend at basin scale (>1 km) and outcrop scale (meters-scale).
893 During subsequent shortening, pre-existing basement structures and rift-related ENE-WW
894 trending fractures are reactivated, so that new fractures are localized above or near
895 reactivated structures at the basin scale. At outcrop scale, new sub-vertical joints formed
896 parallel to the direction of regional compression, though some joints veer towards larger, pre-
897 existing faults.